Department of Bio-Medical Physics and Bio-Engineering

1 4 9 5

UNIVERSITY OF ABERDEEN

COMPARISON OF SENSITIVITY OF PEDRI AND ESR FOR DETECTION OF FREE RADICALS

IJSER

Sunil Laxmanrao Kalagi
B.E. Bio-Medical
Visveswaraiah Technological University,
Belgaum, India.

Supervisor: Prof. David J. Lurie

This report is submitted in partial fulfilment of the requirements for the degree of MSc in Medical Physics at Aberdeen University and is a record of work carried out during Phase III of the Instructional Course for that degree in session 2005/2006.

IJSER © 2018
http://www.ijser.org

*****DEDICATED TO MY PARENTS, SISTERS, WIFE DR.PRARTHANA AND MY KIDS ADITYA -ANISH*****

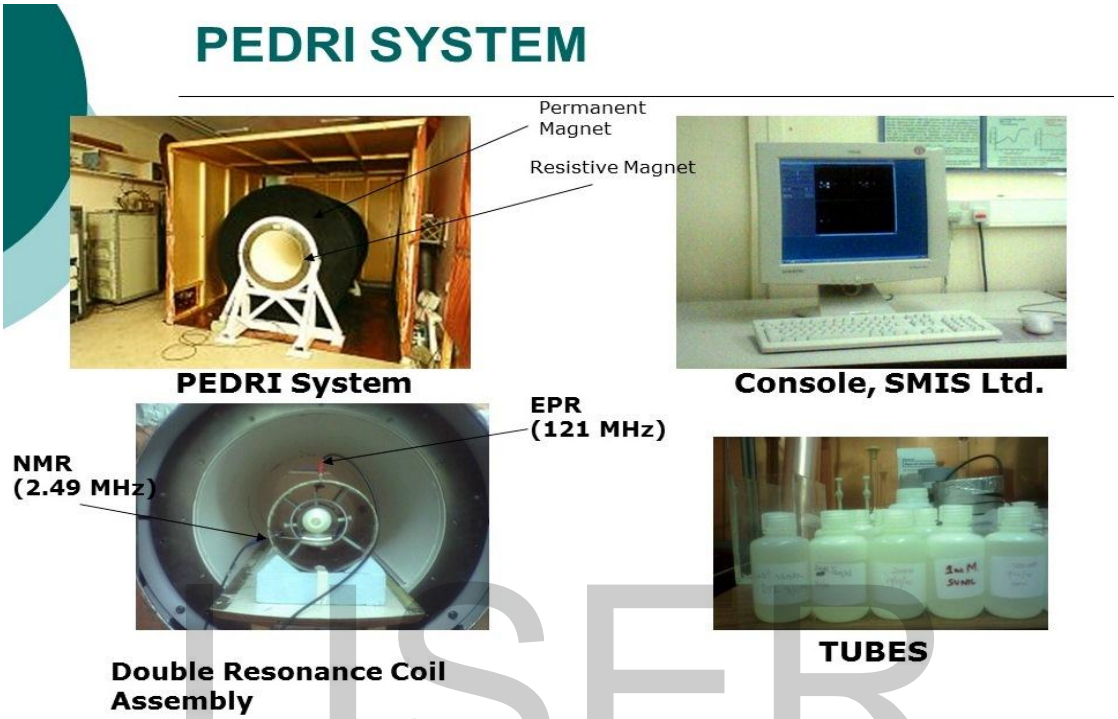

IJSER

IJSER © 2018
http://www.ijser.org

Declaration

This report is my own composition and it has not been accepted in any previous application for a degree. I further declare that except where stated otherwise the work contained in this thesis is original and was performed by myself. The sources of information have been explicitly acknowledged.

Sunil Laxmanrao Kalagi

August 2006

IJSER

IJSER © 2018
http://www.ijser.org

Acknowledgements

I would like to thank my supervisor Prof. D.J. Lurie for his assistance and suggestions throughout this project. Without his advice, enthusiasm and patience, this work would never have been completed. I am also grateful to Dr. Gareth Davies, Mr G.G. Cameron and Miss Rituka Sharma for their valuable advice and many helpful suggestions during composing of my report.

Above all, I am indebted to my family for their understanding and moral support; to them this work is gratefully dedicated.

IJSER

IJSER © 2018
http://www.ijser.org

Abstract

The concentration of naturally occurring free radicals generated in the human body by tissues or cells changes in some diseases. Detection of these free radicals is helpful for diagnosis and treatment of patient. Electron Spin Resonance (ESR) and Proton Electron Double Resonance Imaging (PEDRI) are established methods for detecting free radicals. In this project a X-band ESR spectrometer and a 59 mT PEDRI system were used for detecting free radicals. Experiments were carried out to compare the two systems ability to detect free radicals at different concentrations

Proton-electron double-resonance imaging (PEDRI) is a method for detecting and imaging free radicals in biological samples or animals. PEDRI uses the Overhauser effect, and involves collecting a proton NMR image while irradiating the EPR of the free radical under study. The ESR Bruker system used microwave frequencies to irradiate the sample, while the PEDRI system used frequencies below 300MHz. The ESR irradiation frequency is 660 times the NMR frequency. Using the PEDRI technique the ESR frequency for irradiating the samples was used below 300MHz compared to 9.8GHz used in the ESR Bruker system. A non-imaging variant of PEDRI, field-cycled dynamic nuclear polarization (FC-DNP) spectroscopy allows Overhauser-detected ESR spectra to be obtained via NMR detection. In Field-cycled PEDRI (FC-PEDRI) techniques the magnetic field is switched between two levels during the pulse sequence in order to decrease non-resonant RF power deposition and to increase sensitivity. A spectroscopic version of FC-PEDRI, called field-cycled dynamic nuclear polarisation (FC-DNP) is used to obtain ESR spectra via Overhauser effect.

IJSER

IJSER © 2018
http://www.ijser.org

This project was an attempt to investigate the sensitivity of both the Bruker ESR system and the PEDRI system. The sensitivity of each system was evaluated based on the ability to detect the minimum free radical concentration. From the experiments performed in the project, the PEDRI system was able to detect 20μM Tempol in solution, where as the Bruker ESR system was able to detect 0.01 μM Tempol in solution. The magnetic field of 59 mT was used in PEDRI system and 0.35 T in the ESR Bruker system.

IJSER

IJSER © 2018
http://www.ijser.org

Table of Contents Page No.

IJSER

IJSER © 2018
http://www.ijser.org

IJSER © 2018
http://www.ijser.org

IJSER © 2018
http://www.ijser.org

IJSER

IJSER © 2018
http://www.ijser.org

List of Figures Page No.

IJSER

IJSER © 2018
http://www.ijser.org

IJSER © 2018
http://www.ijser.org

IJSER

IJSER © 2018
http://www.ijser.org

CHAPTER 1 INTRODUCTION

Electron Spin Resonance (ESR) and Proton-Electron Double Resonance Imaging (PEDRI) are non-invasive techniques employed for the detection of free radicals. The electron also has a spin like proton, which gives it a magnetic property. ESR is frequently considered to be in the microwave branch of spectroscopy and NMR is usually classified in radiofrequency spectroscopy. [1] [5]

ESR is a powerful spectroscopic tool that can be used to characterise and detect free radicals or other paramagnetic compounds. In ESR the transitions of unpaired electrons are detected in an applied magnetic field. PEDRI is a double-resonance technique and it is based on the Overhauser effect, which utilises both the ESR and the Nuclear Magnetic resonance (NMR) phenomena in the same sample at the same time to detect and image free radicals. In PEDRI, the ESR resonance of the free radical is irradiated while collecting spectra or NMR images. [5]

IJSER

In this project, the stable nitroxide free radical Tempol is used as a free radical agent to investigate the sensitivity of ESR and PEDRI techniques for detecting the free radicals. In the both techniques different concentrations of Tempol were used to analyse the sensitivity of both techniques. Investigations were carried out on a commercial X-band ESR spectrometer and a home-built PEDRI system.

IJSER © 2018
http://www.ijser.org

1.1Aims and Objective

The main objective of this project is to determine the sensitivity of both ESR and PEDRI systems. A solution of 2mM Tempol is easily detected by both the ESR and PEDRI systems. Experiments were carried out using lower concentrations of Tempol solutions for analysing the free radical sensitivity of both systems. The results obtained from the ESR system are compared with the PEDRI system in terms of SNR. Comparison of SNR (Signal-Noise Ratio) of both systems is done to conclude the sensitivity of the ESR and PEDRI systems.

1.2 Report Structure

The NMR and ESR concept are explained in detail in Chapter 2, which includes the explanations of pulse sequences, gradients, and spin-wrap technique for imaging, which was developed in Aberdeen. It also gives the details of ESR and PEDRI phenomena. This chapter also gives the detail of the Overhauser effect occurring in PEDRI and Field-Cycled Dynamic Nuclear Polarisation (FC-DNP). The ESR and PEDRI hardware systems are explained in Chapter 3. Chapter 4 gives the details of the free radicals used, including the details of preparation of samples with different concentrations and also experimental procedures carried out. Analysis of Results and Discussion are explained in Chapter 5. Chapter 6 gives the overall conclusion of the project.

IJSER

IJSER © 2018
http://www.ijser.org

CHAPTER 2 NMR AND ESR PHYSICS.

Magnetic Resonance is a well known phenomenon explained many years ago and the basis of Nuclear Magnetic Resonance depends on the behaviour of nuclei under magnetic field. Hydrogen nucleus has the highest sensitivity when compared to other elements in the human body. Almost all hydrogen present in the human body is in the form of hydrogen nucleus (1-H) and this is the principal nucleus in NMR for studies and imaging. Under the right magnetic conditions the nucleus goes from one energy state to another energy state, where it emits radiation, which is detected by a tuned coil. [4]

According to Quantum mechanics certain nuclei appear to spin about their axes and this causes them to interact with magnetic fields. Most of the elemental mass is concentrated in the nucleus that consists of protons and neutrons. A 1-H has a single proton and no neutrons. Nuclei with protons and neutrons possess an Intrinsic Spin (I) and can take integer or half integer values. If the intrinsic spin I=0 there is no magnetic interaction. The values of intrinsic spin I depends on the number of protons and neutrons in the nucleus. The hydrogen nucleus with single proton has intrinsic spin value **I**= ½.

IJSER

The intrinsic spin of a nucleus gives rise to angular momentum **P**, which is oriented along the spin axis and is given by,

$$\mathbf{P} = \hbar\mathbf{I} \text{ where } \hbar \text{ is Planck's constant } (\hbar = h/2\pi) \quad \ldots\ldots 2.1$$

The proton of the nucleus possesses electric charge and its rotation results in the formation of an effective current loop and gives rise to an associated magnetic dipole moment μ, as shown in the figure 2.1. The magnetic dipole moment is given in the

IJSER © 2018
http://www.ijser.org

equation form as below:

$$\boldsymbol{\mu} = \gamma P \ldots\ldots\ldots\ldots\ldots 2.2$$

Where γ is the gyromagnetic ratio and is a constant for a given type of nucleus. For protons, $\gamma = 26.75 \times 10^7$ rad s^{-1} T^{-1} or $\gamma/2\pi = 42.58$ MHz T^{-1}.

IJSER

Fig 2.1 The figure above illustrates the mechanism of Nuclear Magnetism. All nuclei with a net spin I show a characteristic magnetic moment μ similar to a dipole, such as a bar magnet with the direction of I and μ oriented along the spin axis. (Copied from reference [13])

The magnetic moment of the nucleus interacts with the applied magnetic field.

2.1 Interaction of the nuclei within a Magnetic field: Quantum Model.

The magnetic dipole moment associated with the nucleus makes it behave like a tiny bar magnet and this makes the nucleus interact with an external magnetic field. According to Quantum mechanics the magnetic moment of a nucleus in an external magnetic field will have (2I + 1) possible orientations corresponding to (2I +1) allowed energy levels. For 1-H (extrinsic spin I = ½) there are two possible

IJSER © 2018
http://www.ijser.org

orientations, either aligned with or against the magnetic field which correspond to low and high energy states respectively as shown in the following figures 2.2a and 2.2b.

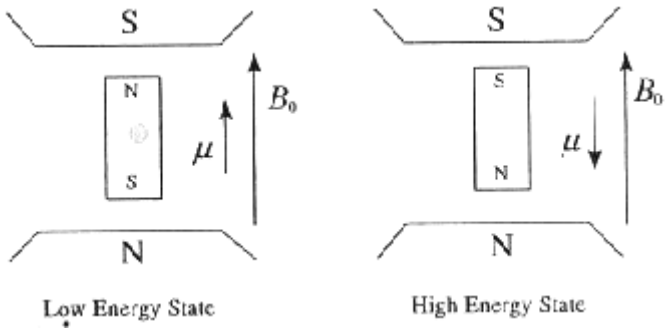

Fig: 2.2 (a) *Fig: 2.2 (b)*

IJSER

The above figure shows the alignment of magnetic moment in a I=1/2 system. Fig 2.2a and 2.2b shows the magnetic moment of nucleus in lower and higher energy states. (Copied from reference [4])

The energy difference ΔE between the two states in the given magnetic field B_0 is given by the following expression:

$$\Delta E = \mu B_0 / I \text{ ……..2.3}$$

Each proton undergoes transition between the two states by the absorption of a photon. The energy E of this photon is directly proportional to its frequency *v* by the Bohr relationship:

$$E = h\nu \text{ ……..2.4}$$

Where h is Planck's constant = 6.620×10^{-34} Js

IJSER © 2018
http://www.ijser.org

The nucleus with spin when placed in an external magnetic field undergoes transition between the two states by absorbing a photon provided with the resonating frequency (energy). The resonance frequency of the nucleus is given by:

$$\omega = \gamma B_0 \text{ or } \omega = \Delta E/ (h/ 2\pi) \ldots\ldots 2.5$$

The spin in the lower energy state and higher energy state have population of N_L and N_U respectively. Although the lower energy level is preferred, thermal motion induces transitions and brings small excess to the lower energy level. The fractional excess of spins in the aligned state given by the following equation:

$$N_L - N_U / N_U = \hbar w_L /kT \ldots\ldots\ldots\ldots 2.6$$

Where k is the Boltzmann constant, w_L is the Larmor frequency and T is the absolute temperature. When the sample is irradiated with electromagnetic energy at the Larmor frequency $w_{L,}$ it induces transition between the two energy states. The electromagnetic radiation of frequency ω can bring about the resonance condition and can flip the orientation of the nuclear spins hence the name Nuclear Magnetic Resonance. As w_L depends on the strength of the magnetic field B_0, the position of the nuclear spins can be mapped to the frequency by the application of magnetic field gradients to the sample and this allows spatial information to be encoded in terms of the frequency and this is the basis of MRI.

2.2 Bulk Magnetisation M

The bulk magnetisation **M** is the combined effect of all the individual magnetic moments observed in the NMR experiment. These individual magnetic moments **μ** make up **M** The individual magnetic moments **μ** are randomly oriented and form the surface of a double cone as shown in the figure 2.3. and on summation creates a net

IJSER

IJSER © 2018
http://www.ijser.org

magnetisation **M** and is given by the vector sum of the individual magnetic moments **μ** i.e. **M** = Σ **μ.**

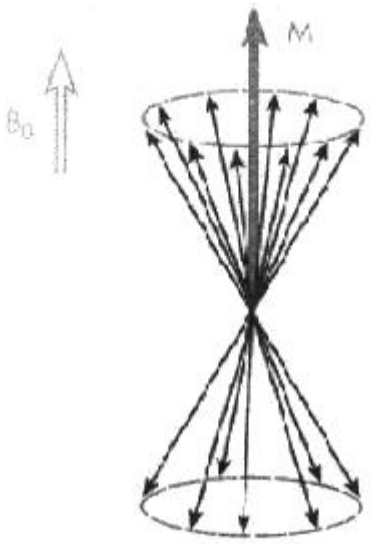

Fig 2.3: The figure above shows the Bulk Magnetisation observed in the NMR. (Copied from reference [13])

IJSER

At equilibrium the bulk magnetisation only has a longitudinal component (i.e. along the B_0 direction). As there is no phase coherence between the individual magnetic moment **μ** that make up **M** at angular frequency w_L, it has only longitudinal component. But there also exists a component of **M** along B_0 due to the tendency of the magnetic moments to align with the applied field. The resultant **M** behaves like a large dipole moment and it is described by the following equation 2.7,

$$d\mathbf{M}/dt = \boldsymbol{w_L} \times \mathbf{M} = \gamma \mathbf{M} \times \mathbf{B_0} \quad \ldots\ldots 2.7$$

On application of electromagnetic radiation to this bulk magnetisation at the resonant frequency of the hydrogen nucleus to this will precess at w_L about B_0 which is explained in the next section.

2.3 NMR Excitation

IJSER © 2018
http://www.ijser.org

Before an NMR signal is detected the bulk magnetisation M must first be perturbed from its equilibrium state. This is done by applying Radiofrequency (RF) pulses at the resonant frequency (Larmor frequency) consisting of a rotatory magnetic field B_1 applied perpendicular to B_0, which tilts away the M from the magnetic field B_0 and execute a spiral path as shown in the figure 2.4. The equilibrium magnetisation then precesses at w_L about the applied magnetic field $\mathbf{B_0}$ as shown in figure 2.4.

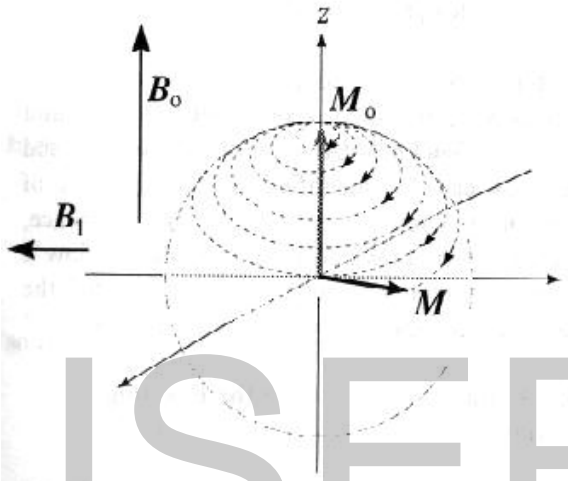

IJSER

Figure 2.4: Spiral path of Bulk Magnetisation after application of RF pulse. (Copied from reference [4])

When the additional magnetic field B_1 is switched off, **M** continues to precess about $\mathbf{B_0}$ and describes a cone at an angle α to $\mathbf{B_0}$ and this angle α is called the flip angle as shown in the following figure 2.5.

IJSER © 2018
http://www.ijser.org

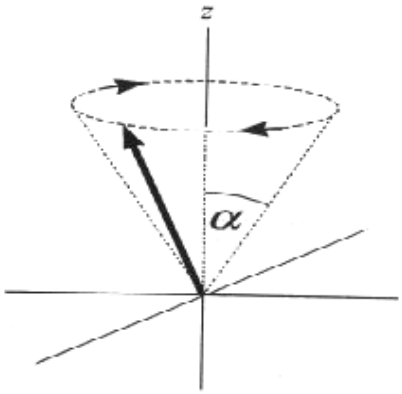

Figure 2.5: M describes a cone of half angle α after B_1 is switched off. (Copied from reference [4])

This flip angle depends on the strength of the applied field B_1 and the time of application of the RF pulse t_p, and the gyromagnetic ratio γ for the nucleus under consideration. The equation for flip angle is given by equation 2.8. If t_p is chosen such that M is tilted through 90^0 then the corresponding RF pulse is called a 90^0 pulse.

IJSER

$$\alpha = \gamma B_1 t_p \quad \text{.....2.8}$$

In NMR detection the sample under study is placed within an RF coil and the RF pulses are generated by applying an oscillating voltage across the terminals of the transmit coil that is tuned to the Larmor frequency w_L . A small voltage is induced in the RF receiver coil by the transverse component of the precessing magnetisation **M** as electromagnetic induction. The RF coil is operated in both transmit/ receive mode. The detected signal is first preamplified as the NMR signal is weak and it is further processed.

Once the RF pulse is switched off the precessing magnetisation relaxes back to equilibrium position $\mathbf{M_0}$ parallel to $\mathbf{B_0}$. Hence the NMR signal decays back when B1 is

IJSER © 2018
http://www.ijser.org

switched off. This type of signal obtained in the absence of B_1 is called a Free-Induction Decay (FID) signal as shown in the following figure 2.6.

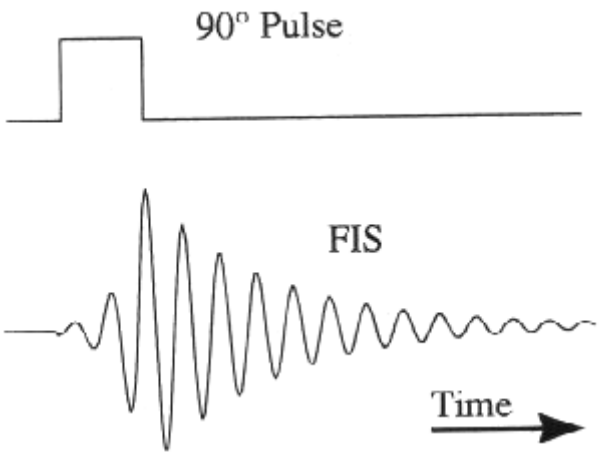

Figure 2.6: Free Induction Signal following 90^0 pulse. (Copied from reference [4])

This spin relaxation is caused by the exchange of energy between spins, and their surroundings, which are explained in the next section.

IJSER

2.4 NMR Relaxation.

One of the most important parameters measured in MRI are Spin-lattice relaxation and Spin-Spin relaxation. Spin-spin relaxation (transverse relaxation) is caused by interactions between neighbouring nuclear magnetic moments characterized by time constant T_2. Spin-lattice relaxation (longitudinal relaxation) is due to the loss of energy from the spins to their surroundings and the time constant is T_1. Both relaxations bring the perturbed magnetisation to the equilibrium position along B_0.

2.5 Measurement of T_1

Inversion Recovery (IR) pulse sequence is used to measure T_1 as shown in the following figure 2.7. The basic IR pulse sequence consists of a 180^0 pulse followed by 90^0 pulse. The timing between these pulses is longer than either of these two pulses as shown in the following figure 2.7.

IJSER © 2018
http://www.ijser.org

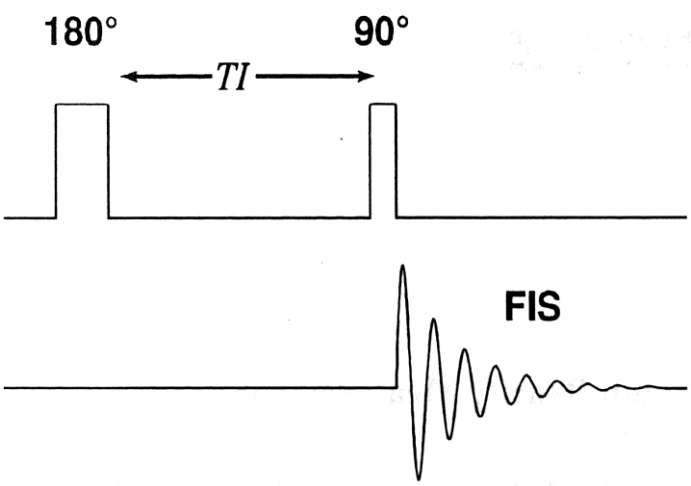

Figure2.7: Inversion Recovery Pulse Sequence. (Copied from reference [4])

The 180^o pulse is used to tip the magnetisation vector so that its magnetisation component M_z has an initial value of –Mo. After 180^o pulse Mz gradually recovers back during the period IR between 180 and 90 pulses. Once the 90^o pulse is applied any Mz component recovered until is converted immediately into transverse magnetisation, which gives the FID. The size of the FID gives the information about how far the magnetisation is recovered towards Mo during the interval TI. The value of the longitudinal component of the magnetisation at a time t after a 180^0 pulse is given by the following expression.

$$M_z(t) = M_0 (1 - 2\exp(-t/T_1))$$

2.6 NMR Imaging.

Magnetic field gradient is just an additional magnetic field in the same direction as Bo (i.e. the z direction), which allows spatial information to be obtained from a sample placed in the imager bore. The amplitude of the gradient field varies linearly along a chosen axis. Hence the gradient makes the magnitude of the main field a linear

IJSER © 2018
http://www.ijser.org

function of position along the chosen axis. If field gradient G_x is in the x-direction, it causes the magnetic field strength to vary according to:

$$B_z(x) = B_0 + x.\ Gx \ldots 2.9$$

NMR imager has three gradient coils to generate gradients along any one of the three orthogonal axes x, y or z which can be thought of as being fixed in the magnet. Hence the gradients along x, y and z direction can be expressed as the following:

$$G_x = dB_z / dx$$

$$G_y = dB_z / dy$$

$$G_z = dB_z / dz \ldots\ldots\ldots 2.10$$

Three main techniques of spatial discrimination are employed in NMR imaging which use field gradients and all the three gradients are combined in the Spin Warp imaging technique. The three main techniques in NMR imaging are as follows:

1. Frequency Encoding
2. Selective Excitation and
3. Phase Encoding. …[4]

The details can be found in the reference 4.

2.6.1 Spin Warp Imaging Technique.

This technique utilises the three methods of spatial discrimination namely selective excitation to define an imaging slice represented by Gs, frequency encoding along a direction in the plane of the slice shown as Gr and phase encoding along the orthogonal direction shown as Gc in fig 2.8. The NMR signal obtained is then subjected to 2DFT methods to obtain an equivalent 2D image. So MRI is based on acquiring 2D information in a selected slice by the application of field gradients and making the individual spin position in the slice a function of position along the field

IJSER

IJSER © 2018
http://www.ijser.org

gradient direction. This technique was developed in Aberdeen in late 1970s, which is almost used by all NMR imagers. [4]

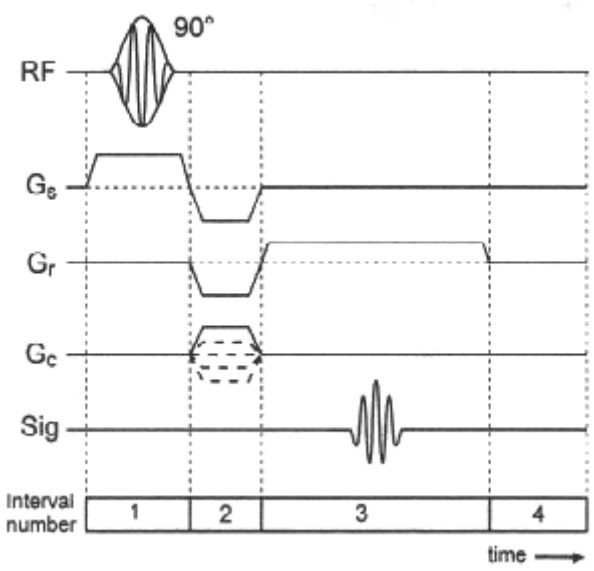

Figure 2.8: Spin warp (2DFT) imaging pulse sequence. (Copied from reference [4])

IJSER

More details of NMR physics can be found in reference [4] and [13].

2.6 ESR Phenomenon.

Electron Spin resonance (ESR) is a form of Magnetic Resonance in which the spin of interest is that of an unpaired electron rather than the nuclear spin which is the case in NMR. The following figure 2.9 shows the magnetic dipoles produced by the electron spins.

IJSER © 2018
http://www.ijser.org

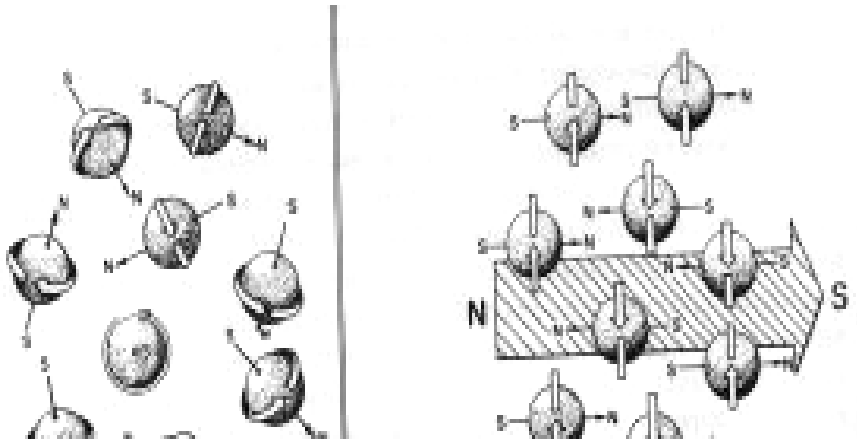

Fig 2.9: Magnetic dipoles produced by the electron spins as though they were not coupled to any other magnetic influences. (Copied from reference [2])

When electrons are paired in chemical bonds or elsewhere their spins are opposed and hence the associated magnetic moments also are opposite and they effectively cancel each other out. But in free radicals the odd electron is not mutually compensated by an orbital partner and the whole free radical will carry an uncanceled electron-spin magnetic moment. Such a molecule is paramagnetic, meaning that it possesses a net electronic magnetic moment. Hence the name EPR and also known as Electron Spin Resonance (ESR) and these two terms can be interchanged.

ESR and NMR are based on the same phenomenon and that is why similar techniques are used for the study of the two spin systems. However, certain differences exist, mainly arising from the fact that the electron's magnetic moment is almost three orders of magnitude larger than that of the proton and the ratio of their gyromagnetic ratios, γ, is equal to $\gamma_e / \gamma_p = 659$. As a result, the frequency of the pulse that is needed to excite an electron spin system does not lie anymore in the radiofrequency region (MHz), as for the nuclear spin, but in the microwave region (9 GHz) for an equivalent applied magnetic field strength 0.35T.

IJSER

IJSER © 2018
http://www.ijser.org

2.7.1 ESR Spectroscopy Theory

EPR spectroscopy is a technique that permits the detection and, in favourable cases, the characterisation and, where possible, the identification of molecules with unpaired electrons without altering or destroying the molecules or in other words it is concerned with the resonant absorption of microwave radiation by paramagnetic samples in the presence of an applied magnetic field.[1]

According to the principles of quantum mechanics, every molecule or atom has discrete states, each with a corresponding energy level. Spectroscopy is the measurement and interpretation of the energy level differences between the atomic or molecular states, which can provide information about the identity, structure, and dynamics of the sample under study.

The energy differences can be measured by experiments based on Planck's law. If a molecule or atom is irradiated by electromagnetic radiation, absorption will take place if

$$\Delta E = h\, v_0 \text{……..2.14 [2]}$$

Where ΔE is the energy difference of two energy levels, h is Planck's constant and v_0 is the frequency of the electromagnetic radiation needed to bring about the transition between the low and the high energy states.

2.7.2 The Zeeman Effect and Resonance Phenomenon.

A shift in the energy levels of an isolated atom or molecule as a consequence of an external magnetic field is called the Zeeman Effect. [12] These energy differences are studied by EPR spectroscopy and are mainly based on interactions of unpaired electrons in the sample with a magnetic field produced by a magnet. The electron due

IJSER © 2018
http://www.ijser.org

to its magnetic moment will have two states in the presence of a magnetic field. The state of highest energy when the electron's magnetic moment, μ is parallel to the magnetic field and a state of lowest energy when μ is aligned against the magnetic field. The two states are characterised by the projection of the electron spin on the direction of the magnetic field. As the electron has a spin of 1/2, in the parallel state the spin's projection will be –1/2 and in the anti parallel state 1+1/2 (Also see figure 2.11). Quantum mechanics provides the basic EPR equation given by the equation 2.15. [17]

$$E = +/- \tfrac{1}{2} g \beta B_0 \ldots\ldots 2.15$$

Where E is the energy of the corresponding spin state, g is known as the g-factor and is approximately equal to 2 for free radicals [5], β is a fundamental physical constant known as the Bohr magneton which describes the magnetic moment of the spin system in terms of properties like mass and charge, and B_0 is the applied magnetic field strength in Tesla. The equation giving the energy difference between the excited and the ground state in this case is

$$\Delta E = g \beta B_0 \ldots.. 2.16$$

The following figure 2.14 shows the energy levels of an electron in a magnetic field.

IJSER

IJSER © 2018
http://www.ijser.org

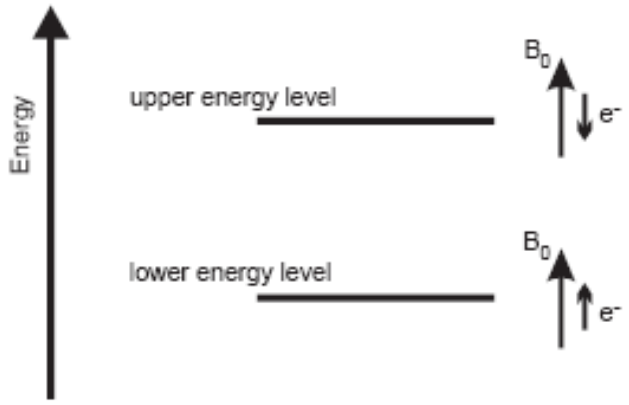

Fig 2.10: Two possible states of an electron in a magnetic field. Lower energy level corresponds to the electron "spin" being parallel to the direction of the applied magnetic field, while its orientation is reversed in the upper energy level, as shown by the arrows on the right. (Copied from reference [5])

From equation 2.14 and 2.16, we can derive the expression for the frequency v_0 which satisfies the resonance condition. [5]

$$h\, v_0 = g\beta\, B_0 \quad \text{.....2.17}$$

IJSER

Since any physical system prefers to be in lower energy state, the electrons jump back to lie in alignment once again with the applied magnetic field. In this process they give up their excess energy absorbed during excitation by re-emitting EM radiation at the same frequency. This is known as the 'resonance' condition in which the magnetic dipole of the molecule interacts with the magnetic component of a radiation field and hence absorption is observed in the presence of a static magnetic field. This process occurs during a characteristic time known as electron relaxation time T_1 which is typically between 0.1 μs and 1μs. [5]

IJSER © 2018
http://www.ijser.org

In EPR spectroscopy we take advantage of these phenomena and, keeping the frequency of the electromagnetic radiation constant, we sweep the magnetic field until the resonance condition is reached. This approach looks strange instead of keeping the magnetic field constant and sweeping the frequency, but it is dictated by limitations of microwave electronics. At the frequencies used in most EPR spectrometers, it is necessary to hold the sample in a tuned cavity (See section 3.1.2). It is this which requires that the field rather than the frequency is swept, since it is impossible to retune the cavity continuously. [17]

2.7.3 Hyperfine Interactions

The magnetic moment, often possessed by a nucleus of an atom in a molecule or complex, produces a local magnetic field which can be sensed by the electron. The interaction between the electron and the nucleus is known as ‘hyperfine interactions’ [5]. It is called ‘hyperfine’ rather than ‘fine’ for historical reasons, as fine coupling refers to the splitting caused by the interaction of two or more unpaired electrons. The identity and number of atoms which make up the molecule or complex and their distances from the unpaired electron and other useful information can be provided through observation of this interaction.

IJSER

The origin of hyperfine interaction lies in the fact that the magnetic moment of the nucleus produces a magnetic field at the electron in addition to the external magnetic field supplied by the experimenter. The magnitude of this local field is small since the nuclear magnetic moment is much smaller than that of the electron. Depending on the nuclear magnetic moment alignment, this additional field opposes or adds to the applied magnetic field the electron experiences, to reveal the Zeeman Effect.

A single isolated unpaired electron would give a single EPR absorption signal. If a spin ½ nucleus, such as a hydrogen nucleus, was in the immediate environment of the

IJSER © 2018
http://www.ijser.org

unpaired electron this would give an EPR spectrum where the single signal (line) would be split into two signals (lines) each one away from the original signal by the additional magnetic field due to the nearby nucleus. If, however, the nearby nucleus was nitrogen, having spin equal to 1, the electron would experience three energy levels, so would give a triplet signal. The following figure 2.11 shows the energy level splitting in the absence and in the presence of an applied magnetic field and also a typical ESR spectrum obtained by sweeping the magnetic field.

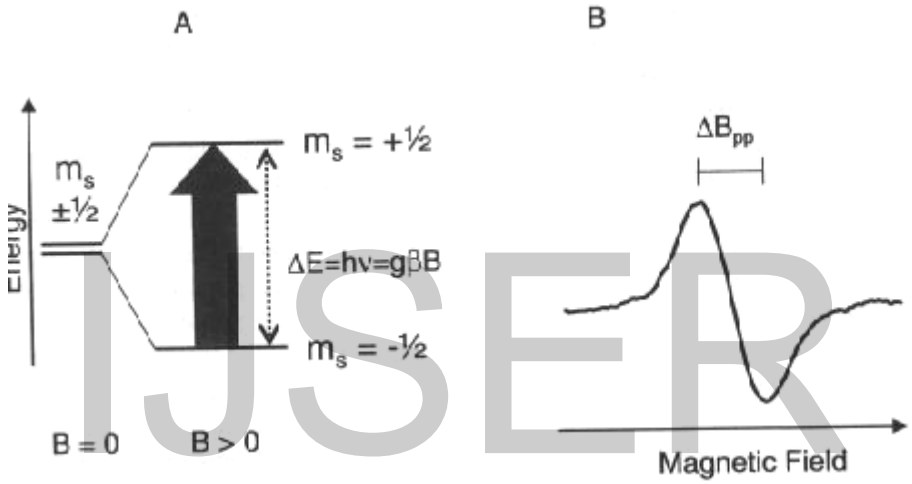

Fig 2.11: (A) Energy level splitting of spin population in presence of applied magnetic field only and in presence of applied magnetic field and with interaction with a nuclear spin ½ spin. (B) A typical first derivative EPR spectrum is shown with peak-to-peak line width definition. The spectrum is obtained by sweeping the magnetic field while the sample is exposed to fixed-frequency radiation. (Copied from reference [1])

The nitroxide free radicals used in this study give 1:1:1 triplet signals. In that case, the hyperfine splitting arises from the interaction between the nuclear spin of the Nitrogen atom and the electron spin of the free electron associated with the N-O bond. It has already been mentioned that the interaction between the Nitrogen nucleus of spin one

IJSER © 2018
http://www.ijser.org

and the electron of spin one-half results in three EPR lines in the presence of a magnetic field. However there is a further hyperfine interaction between the electron spin and the hydrogen nuclei in nitroxide free radicals resulting in each of the three lines being split, with the number of lines depending on the number of neighbouring hydrogen nuclei and their relative contribution. Nevertheless, in most cases the additional lines are unresolved and the EPR spectrum consists of three single lines, which are shown, in figure 3.6.

2.7.4 Signal Intensity.

Other quantitative results in EPR spectroscopy come from the measurement of the concentration of the EPR active species in the sample under examination. The size of the absorption peak is directly related to the number of spins in the sample. The signal size can be measured either as the peak-to-peak height of the absorption line or as the integrated intensity, i.e. the area under the absorption curve. The former is commonly preferred, as the latter requires a good signal to noise ratio and a flat baseline.

IJSER

Quantitative work in EPR spectroscopy is done through comparisons between the acquired spectra. These comparisons will only be valid if the line shapes are identical between the different samples. This again means that the conditions and the instrument settings during the spectra acquisition must be identical so that we end up comparing “like with like” spectra.

2.7.5 X-band EPR

Generally the resonance equation 2.17 can be satisfied for any frequency of electro-magnetic radiation. However, the population difference between the two energy levels

IJSER © 2018
http://www.ijser.org

allowed for the electron spin states increases linearly with the applied magnetic field strength. Thus for reasons of sensitivity we need to use a frequency as high as possible. Limitations at the high frequency end include sample size, geometry, magnetic field intensity, and homogeneity. Most commercial EPR spectrometers operate in the microwave region, primarily at X-band region i.e. f = 9 –10 GHz. This X-band radiation has a wavelength of approximately 3 cm. The spectrometer used for this study was operating at these frequencies .

2.8 PEDRI

Proton Electron Double Resonance Imaging is based on the Overhauser effect also known as Dynamic Nuclear Polarisation (DNP). It was predicted by Overhauser (1953) and experimentally verified by Carver and Slichter (1956). PEDRI was first demonstrated in the Biomedical Physics Department (Aberdeen University) in 1987 using a whole body resistive magnet system working at 40mT. [5] [6]

IJSER

In DNP the EPR resonance of the solute is irradiated and under right conditions there is transfer of polarisation from the electrons to the protons which results in the enhancement of the signal also called Overhauser Enhancement. PEDRI is the imaging version of this technique, wherein using magnetic field gradients uses the NMR signals to generate an image. The NMR signal is enhanced in parts of the sample where the free radicals are present due to DNP and hence provides information about the distribution of the free radical in the sample. [1]

2.8.1 Dynamic Nuclear Polarisation

The molecules in free radicals contain unpaired electrons and hence possess a net electron spin ‘S’. These electron spins interact with the nuclear spins ‘I’. The

IJSER © 2018
http://www.ijser.org

interaction between these spins due to random molecular motion will ensure that each nucleus is in constant interaction with an unpaired electron during its period of relaxation. Considering only pairs of electron and nuclear spins so that I =1/2 and S=1/2, there are four possible energy levels and each proton-electron pair can be represented by m_s, m_1 where m_s and m_1 are magnetic spin quantum numbers.

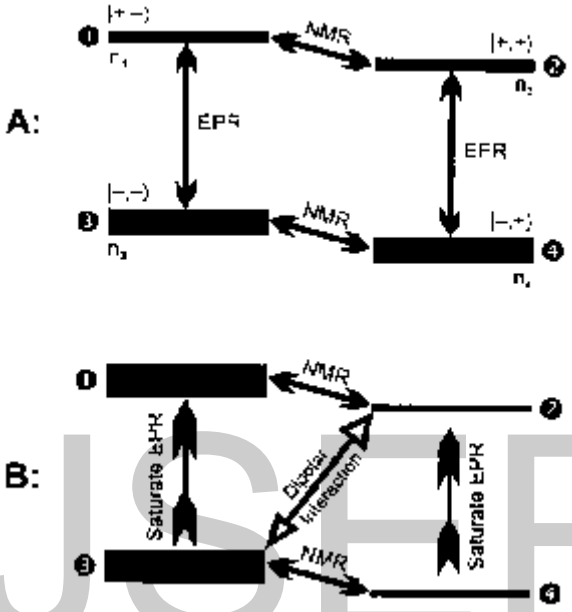

IJSER

Fig 2.12: Energy Level Diagram for the two-spin nucleus-electron system and phenomological description of the Overhauser effect. (A) At thermal Equilibrium (B) while saturating EPR transition. (Copied from reference [4])

The four energy levels can be represented as $|+-\rangle, |++\rangle, |--\rangle, |-+\rangle$ in order of decreasing energy and the energy level diagram is as shown in figure 2.12. The energy difference between the states 1 and 3 and 2 and 4 (EPR transitions) is about 660 times that between 1 and 2 and 3 and 4 (NMR transitions). Each energy level population is represented by n_i and the thickness of each line is proportional to the population. The population in each state at thermal equilibrium obeys the Boltzmann distribution as shown in fig 2.12(A). At Level 1 the NMR spins are in the higher

IJSER © 2018
http://www.ijser.org

energy state and has the lowest population, while level 4 has the highest. The difference in energies involved in electron transitions is much greater than that in NMR, this being the reason for the much smaller difference between the populations of states 1 and 2 as against 1 and 3 as seen in the above figure 2.12.

Fig 2.12(B) shows the situations when the electron transitions i.e. 3 ↔ 1 and 4 ↔ 2 are irradiated. If the intensity of EPR irradiation is sufficient then the EPR transitions will be saturated causing an equalising of population states n1 = n3 and n2= n4 but rapid molecular motion in the free radical solution cause a dipole-dipole interaction between nuclear spins and unpaired electrons and this causes a simultaneous flipping of both nuclear and electron spins. This is called the cross relaxation pathway and is shown in fig 2.12(B) between states 2 and 3. It's this interaction that restores the relative populations of these states to the Boltzmann levels and because the energy difference between the states 2 and 3 for example is much larger, the polarisation is large as can be seen in Fig 2.12(B), n3>> n2. The difference in populations between the nuclear states 1 and 2 is also greater in comparison to the state at thermal equilibrium as shown in fig 2.12(A). As the difference in polarisation of the nuclear states 1 and 2 is similar to that exhibited by the electron states we say that there is a transfer of polarisation from electrons nuclear spins. This transfer of polarisation results in the Overhauser enhancement observed in the NMR signal that is recorded. The level of enhancement however varies with the power of EPR irradiation and the NMR signal amplitudes for different power levels are shown below in figure 2.13. [1]

IJSER

IJSER © 2018
http://www.ijser.org

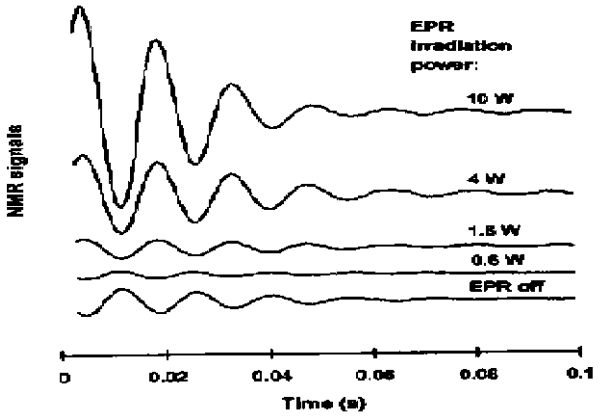

Fig 2.13: The figure shows the DNP NMR FID's obtained at a field strength of 10mT at different irradiation power. (Copied from reference [4])

As can be seen in the energy level diagram Fig 2.12(B) the population of the higher energy state 1 and 3 exceeds that of the lower energy state 2 and 4. This population reversal upon irradiation causes the phase change in the NMR signal. It is important to note that there could be dipole-dipole interaction between 1 and 2, 3 and 4, 1 and 4, but the transitions between 2 and 3 dominate. Taking into consideration all these transitions the maximum possible enhancement factor of the NMR signal can be shown to be ½ ratio of the gyro magnetic ratios for electron and proton, i.e. –329. [1]

IJSER

2.8.2 Enhancement Factor

The enhancement factor E can be defined as the ratio I_z / I_0, where I_z and I_0 are the NMR signal amplitudes with and without EPR irradiation. It can be written as in the following equation 2.17. [1]

$$E = 1 - \rho f s \left| \frac{\gamma_s}{\gamma_I} \right| \quad \text{.....2.17}$$

IJSER © 2018
http://www.ijser.org

ρ is the coupling factor, which depends on the nature and time dependence of the nuclear-electron interactions. Where γ_s and γ_I are the electron and nuclear gyro-magnetic ratios and *f* is the leakage factor. In case of purely scalar interactions ρ takes the value of –1, while ρ = ½ if the interactions are dipolar. Due to the random motion of the solute particles the dipolar interactions dominate and ρ can be taken to be independent of the type of free radical and can be taken to be ½. *f* is the leakage factor and is a measure of the fraction of nuclear relaxation arising from the interactions with the free radicals unpaired electrons in solution. It can be written as:

$$f = 1 - \frac{T_1}{T_1^0} \quad \text{……..…2.18}$$

Where T_1 is the NMR spin relaxation time of the free radical and T_1^0 is the NMR spin lattice-relaxation time of the solution in the absence of the free radical. The saturation factor is a measure of the degree of saturation of the EPR resonance and it depends on the RF field B_2 produced by the EPR transmit coil and the unpaired electron's EPR relaxation times, τ_1 and τ_2. The saturation factor can be written as:

$$s = \frac{\gamma_s^2 B_2^2 \tau_1 \tau_2}{n(1+\gamma_s^2 B_2^2 \tau_1 \tau_2)} \quad \text{……..…….2.19}$$

Where n is the number of lines in the free radical's EPR spectrum. For ρ = ½ and for proton NMR (with $|\gamma_s| / |\gamma_I|$ = 658), and on rearranging the equations 2.17, 2.18 and 2.19 we get the following expression.

$$E = 1 - \frac{329}{n\left(1+\frac{1}{\alpha\rho}\right)\left(1+\frac{1}{kcT_1^0}\right)} \quad \text{……..2.20}$$

IJSER

IJSER © 2018
http://www.ijser.org

The first two terms in the denominator are the reciprocal of the saturation factor and can be written in terms of power by assuming that $B_2^2 \alpha P$, where P is the power of the EPR irradiation. α is a constant of proportionality depending on the sample's EPR relaxation time and the characteristics of the EPR resonator. The second term in the denominator is the reciprocal of the leakage factor, which has been rewritten in terms of the concentration c, of the free radical solute and its longitudinal NMR relaxivity k, this is the term that determines the DNP response as a function of the concentration of the free radical. [1]

2.8.3 PEDRI technique and Pulse sequences.

The PEDRI technique involves EPR irradiation followed by NMR excitation. The PEDRI pulse sequence is usually applied as an interleaved sequence with each alternate NMR excitation being preceded by EPR irradiation at the chosen frequency, as shown in the following figure 2.14. After the signal acquisition is complete the with-EPR and without- EPR NMR data are subtracted and a difference image is generated which shows the free radical distribution in the sample as regions of non-zero intensity. In PEDRI the full complex data sets are subtracted to preserve the NMR signal phase change that occurs upon EPR irradiation.

IJSER

IJSER © 2018
http://www.ijser.org

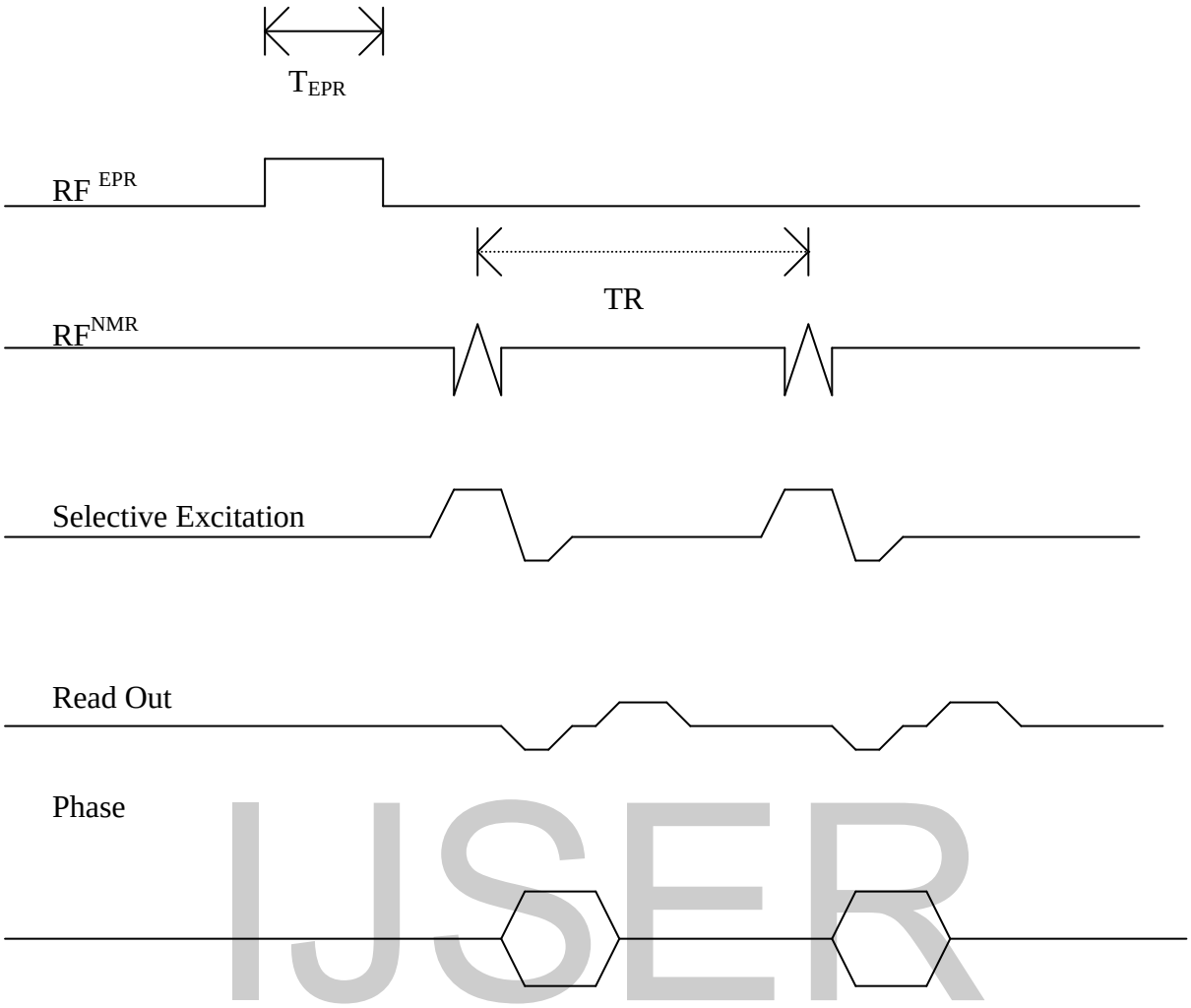

IJSER

Fig 2.14: Basic PEDRI pulse sequence which allows to collect 'with EPR' and 'without EPR' images.

For optimum DNP effect, the EPR irradiation time T^{EPR} should be at least $3xT_1$. The T_1 here is the NMR longitudinal relaxation time of the sample. The total image acquisition time for an N x N pixel image is 2NxTR where TR is the pulse sequence repetition time. PEDRI provides useful information about free radical distribution in the sample of interest but with increasing frequency of EPR irradiation the specific absorption rate (SAR) also increases which is explained in the immediate next section.

IJSER © 2018
http://www.ijser.org

2.8.4 Specific Absorption Rate (SAR).

SAR is defined as the RF power absorption per unit body mass and has units Watt/kg. When magnetic fields of frequency exceeding about 100 kHz are applied to electrically conductive tissues in the body then eddy currents are set up and due to the resistive impedance in the patient RF power deposition occurs. The power deposition P for a conducting sphere of radius a and resistivity ρ placed in a uniform RF magnetic field of angular frequency ω and amplitude B_1 is given by the following equation 2.22.

$$P = \frac{\pi\omega^2 B_1^2 a^5}{15\rho} \quad \ldots\ldots 2.22$$

IJSER

The power absorption per unit mass or SAR increases as a^2 since the mass increases as a^3. It has been shown that the resonant power deposition in a conducting sample increases as the square of the irradiation frequency which in turn is proportional to the magnetic field strength at which EPR irradiation occurs. The best way to handle this problem is to reduce the magnetic field strength at which the EPR irradiation takes place. An alternative method would be to reduce the EPR irradiation duty cycle (EPR ON / EPR OFF) thereby reducing the mean absorbed power. The first method is however the essence of field-cycled PEDRI or FC-PEDRI. [Redpath et al 1984 (14)]

2.8.5 Field-cycled PEDRI

The SAR could be lowered by performing the PEDRI experiments at very low magnetic fields thereby lowering both the EPR and the NMR irradiation frequency. But this would affect the signal-to-noise ratio of the MRI experiment and would also

IJSER © 2018
http://www.ijser.org

affect signal sensitivity and image quality. FC-PEDRI overcomes the power deposition and SNR problems by switching the applied field B_0 between levels during the pulse sequence as shown in figure 2.15. So the EPR irradiation occurs during the lower field and the B_0 field is then restored to its higher level at which the NMR detection takes place and this ensures that the SNR remains unaffected.

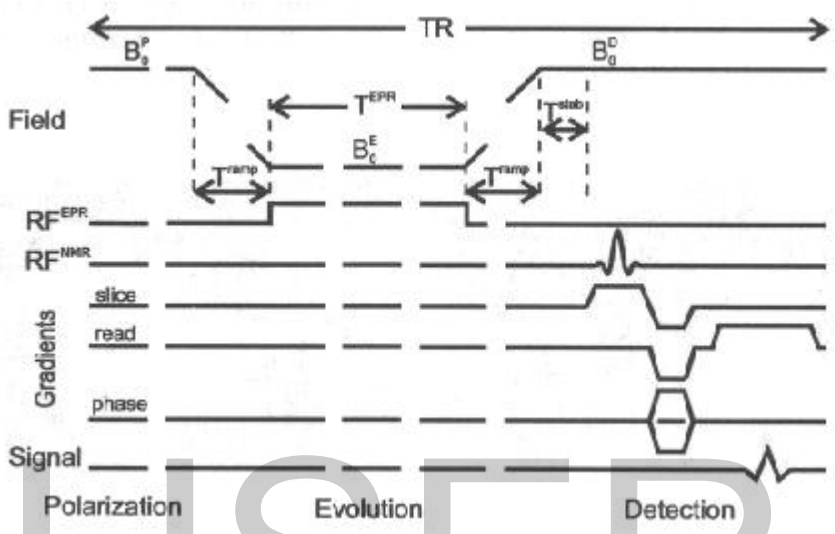

Fig2.15: FC-PEDRI pulse sequence. (Copied from reference [1])

IJSER

The pulse sequence can be divided into 3 different periods namely polarisation, evolution and detection and B_0^P, B_0^E, B_0^D (Noack, 1986) being the magnetic field strengths during each of these periods. In FC-PEDRI the B_0^P and the B_0^D are usually the same and as high as the hardware will allow in order to achieve a high SNR. The EPR irradiation is applied during the evolution period thus reducing the EPR irradiation frequency and limiting the RF power deposition to safe limits. But at the same time DNP enhancement is maintained. The timing of the pulse sequence is also a crucial factor that determines the sensitivity of the technique. The EPR irradiation time T^{EPR} should be three times the NMR longitudinal relaxation time i.e. 3x T_1 at the field B_0^E to for maximum DNP effect. The other important parameter is the time delay between the end of the EPR irradiation and the application of the NMR detection

IJSER © 2018
http://www.ijser.org

pulse which is shown in figure 2.15 as the sum of the field cycling ramp time T^{ramp} and the field stabilisation time T^{stab}. The total time delay should be less than T_1 at B_0^E in order to ensure that the proton magnetisation does not decay significantly before measurement of the signal.

2.8.6 FC-DNP Spectroscopy.

The determination of B_0^E is important for collecting the images of free radical sample and it is the value corresponding to one of the EPR resonances. It is the value around which the electron-proton polarization occurs and operating the FC-PEDRI pulse sequence using this B_0^E value allows to get appropriate images. The FC-DNP pulse sequence shown in fig 2.16, is used to determine the B_0^Eevolution field strength for the sample under study. FC-DNP pulse sequence is basically an FC-PEDRI NMR pulse sequence without the magnetic field gradients. FC-DNP spectroscopy can also be observed as a to obtain ESR spectroscopic information via the Overhuaser effect. To record the FC-DNP spectrum of the free radical of interest the pulse sequence is repeated a number of times while the evolution field B_0^E is incremented in small steps with each repetition. [5]

IJSER

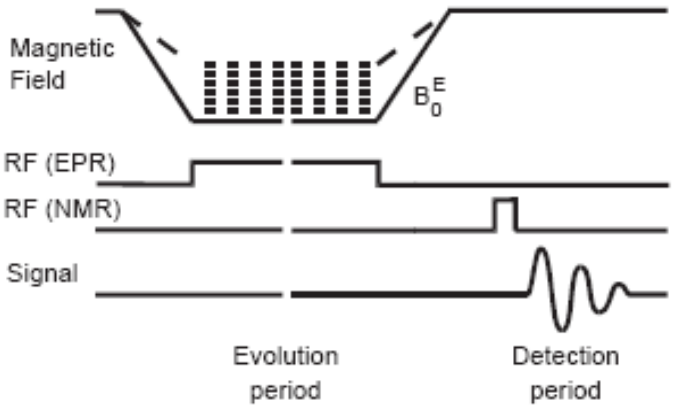

Fig 2.16: FC-DNP pulse sequence. (Copied from reference [5])

IJSER © 2018
http://www.ijser.org

FC-DNP spectrum is acquired (see figure 2.20) by irradiating the sample at a constant frequency and power. The FC-DNP spectrum is plot of the NMR signal amplitude vs B_0^E as shown in the figure 2.17.

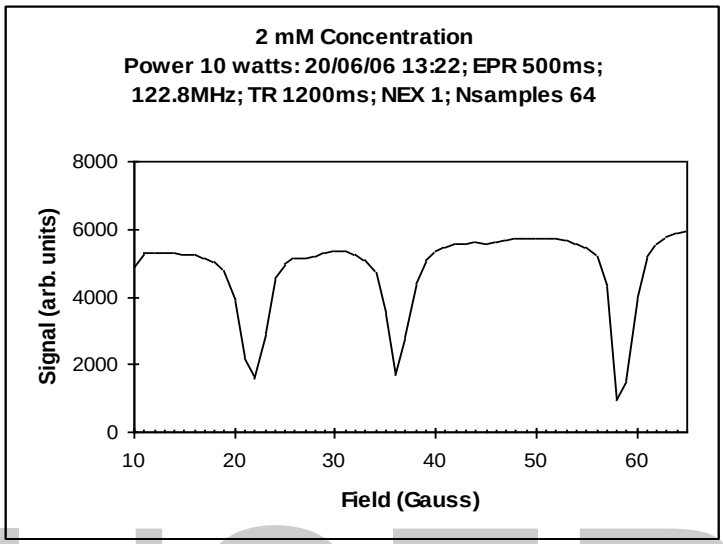

Figure 2.17: FC-DNP spectrum of a 2mM TEMPOL sample, showing three ESR lines at 22G, 37 G and 58G.

IJSER

The FC-DNP spectrum gives the free radical's EPR resonances with relative intensities, which are modulated by the electron-proton interactions and may not be the true EPR intensities. The evolution field parameter of the FC-PEDRI NMR pulse sequence shown in fig2.15 is then changed to the B_0^E that has been determined and the PEDRI images are then collected as a set of three images namely, the without –EPR image, with –EPR image and the difference image of these two images that shows the distribution of the free radical in the sample.

IJSER © 2018
http://www.ijser.org

CHAPTER 3 ESR AND PEDRI HARDWARE DESCRIPTION.

3.1 ESR System

Figure3.1: Picture showing Bruker ESR system.

IJSER

Any spectrometer involves three basic elements, namely a radiation source, a sample which absorbs some of the radiation and a detector which measures the intensity of transmitted radiation. The ESR system used in this project is shown in the figure 3.1. It is a commercial spectrometer, manufactured by the company Bruker. It comprises an ER 200 spectrometer together with an ESP 300 computer system, for spectrometer control and data acquisition. In an X-band EPR spectrometer the radiation source is a klystron, giving an output in the microwave region (9-10 GHz frequency). Microwaves from the klystron are transmitted to the sample through a microwave waveguide. The sample is held in an external magnetic field. The intensity of transmitted microwaves is determined by a microwave rectifier, usually a silicon crystal, which proportionately converts the microwave radiation to an electrical

IJSER © 2018
http://www.ijser.org

current that can be accurately measured. The figure 3.1 shows the picture of Bruker ESR system used in the project. [2]

The basic block diagram of the ESR system is as shown in figure 3.2. In this instrument the electromagnetic radiation source and the detector are in the microwave bridge. The sample is placed in the microwave cavity as shown in figure 3.3, which amplifies the weak signals from the sample. A resistive magnet of 0.35 Tesla (Note: One Tesla = 10000 Gauss) is used in the ESR experiment. The signal processing and control electronics are inside a console and the whole operation is controlled via a computer which is used for analysing data and for the co-ordination of all the units during the acquisition of a spectrum.

IJSER

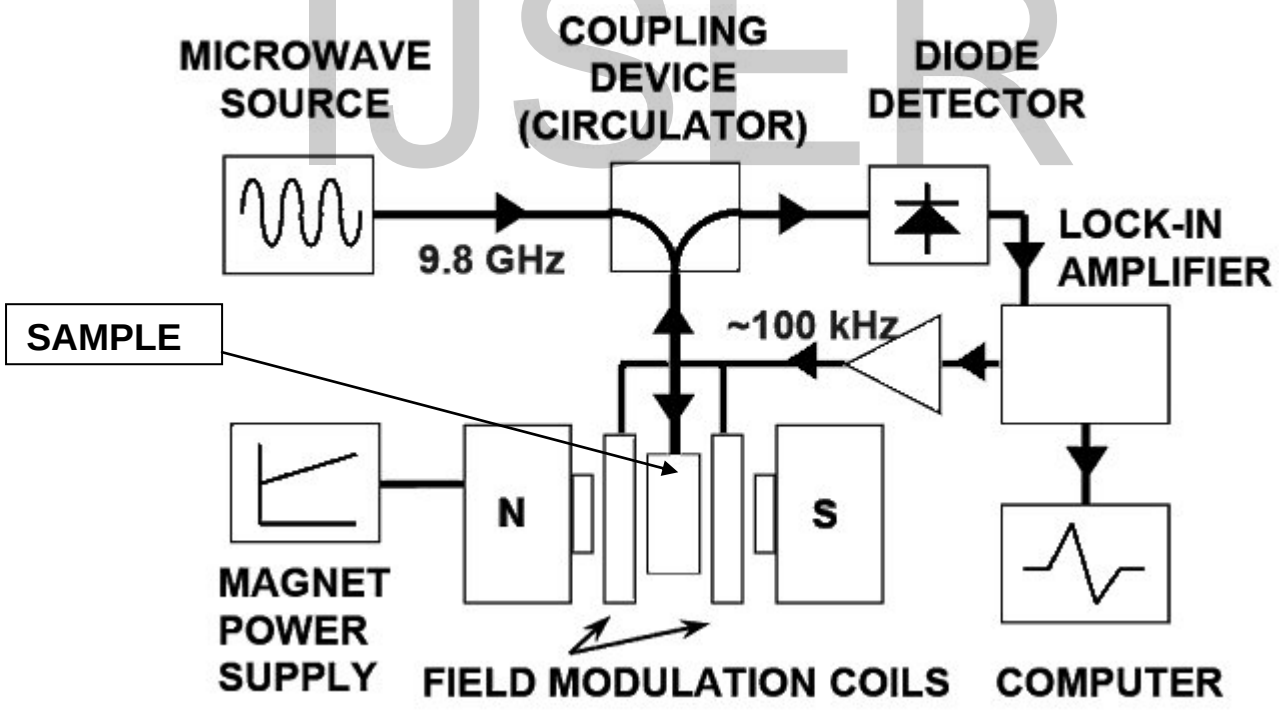

Fig 3.2: ESR system block diagram. (Copied from reference [16])

Since the reflected signal on resonance is small, magnetic field modulation coils are used to improve the signal-noise ratio. The major components of the EPR spectrometer are described in detail in the following section.

IJSER © 2018
http://www.ijser.org

3.1.1 Microwave Generator

The microwave bridge houses the microwave source and the detector. The microwave source is a klystron which is an electronic valve oscillator. The EM wave produced in the klystron passes from a variable attenuator through which we can accurately control the microwave power irradiating the sample.

An attenuator is a circuit element that, when inserted between generator and a load, reduces the amplitude and changes the phase of the radiofrequency signal incident on the load. The microwave power is reduced from the value P_1 in the absence of the attenuator to the value P_2 when it is in place. This reduction in power is measured by a quantity called the attenuation A, which is defined by

$$A = 10 \log_{10} \left(\frac{P_1}{P_2} \right) \text{.....3.1}$$

It is expressed in the units of decibels (dB). This expression assumes that both the generator and load ends of the transmission line are terminated in matched impedances.

IJSER

The Bruker spectrometer, like most EPR spectrometers, is a reflection spectrometer that measures the amount of the radiation reflected from the tuned cavity containing the sample. A circulator transmits power from one terminal to the next in sequence, allowing us to isolate the microwave radiation coming back from the cavity.

Detection of this signal is by biased Schottky barrier diode. It does this by converting the microwave power to an electrical current. Optimal sensitivity and ability for quantitative signal intensity measurements are achieved when the diode operates in its linear region. For the instrument we used, the detector current should be approximately 200mA.

IJSER © 2018
http://www.ijser.org

3.1.2 The EPR Cavity

The ER 4103 TM cylindrical microwave cavity was used in the project for performing the ESR experiments. The TM stands for transverse magnetic waves. The TM_{mnp}, where the subscripts m, n and p are the number of half-cycle variations in the angular (Φ), radial (r) and longitudinal (z) directions, respectively. [Poole] Figure 3.3 shows the cylindrical cavity used in the project. The cylindrical cavity is particularly useful for examining samples with high dielectric loss.

IJSER

Figure3.3: A cylindrical TM_{110} cavity. (Copied from reference [20])

The ER 4103 TM is a TM_{110} cylindrical cavity with a nominal centre frequency of 9.8 GHz. The figure 3.4 shows an example of transverse magnetic wave configuration in TE_{112} cylindrical resonant cavity. The maximum sample diameter of 17mm can be used and is designed to accommodate specially for wide flat cells for aqueous solution studies. It provides signal increase compared to other standard cavity due to the larger sample volume, which can be accommodated in the TM flat cells. [21]

IJSER © 2018
http://www.ijser.org

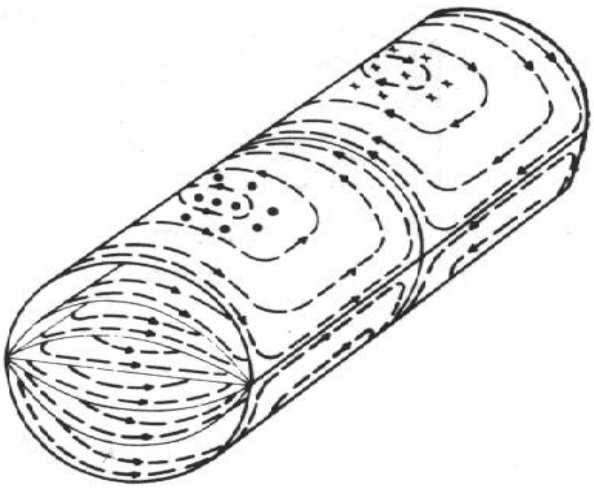

Figure 3.4: Transverse magnetic wave configuration in TE_{112} cylindrical resonant cavity. (Copied from reference [3])

The coupling of the microwaves to the cavity is achieved by adjusting an iris, which is a passage of adjustable dimensions at the border between the wave guide and the cavity as shown in figure 3.5. The size of the iris controls the amount of microwaves reflected back from the cavity and that entering the cavity by matching the impedance of the waveguide and the cavity. The matching is done by adjusting an iris screw either manually or via the console. An EPR signal is generated when the cavity coupling changes as a result of an absorbing sample. The cavity, in that case, is no longer critically coupled and microwaves are reflected back to bridge. Critical coupling is re-achieved by means of the iris screw.

IJSER

IJSER © 2018
http://www.ijser.org

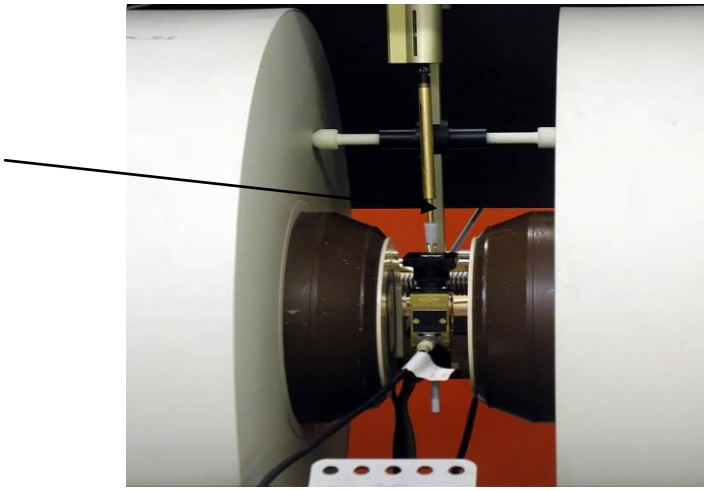

Figure 3.5: The arrow mark pointing towards the IRIS coupler.

3.1.3 The Signal Channel

The signal channel is a unit housed in the console, provides the means for phase sensitive detection via a technique that enhances the sensitivity of the spectrometer.

IJSER

The technique involves the sinusoidal modulation of the magnetic field strength at the modulation frequency, which can be chosen by the operator. In the event of an EPR signal, part of the signal is swept and the reflected microwaves are modulated in amplitude at the same frequency. The signal channel produces a DC signal proportional to the amplitude of the modulated EPR signal, compares it with a reference signal of the same frequency and accepts only the signals that match. A time constant is used to filter out more of the noise. An EPR signal approximately linear over an interval as wide as the modulation amplitude is transformed into a sine wave. The amplitude of that sine wave is proportional to the slope of the signal. Therefore what we get as an EPR signal is the first derivative of the absorption line(s) as shown in the figure 3.6.

IJSER © 2018
http://www.ijser.org

The signal channel incorporates an integrating ADC (Analogue to Digital Converter) to transfer the analogue EPR spectra to the digital data acquisition system. The integration method for the conversion integrates the noise out of the signal. The noise diminishes as the square root of the conversion time and the whole effect is independent of the time constant of the signal channel.

Figure3.6: Typical spectrum observed in the Bruker ESR system.

The digital data representing the analogue EPR spectrum can be stored, after their acquisition and transformation, either to the hard disc of the computer that runs the whole system or to a floppy disc. The data are then available for further manipulation in the future. Another option is the digital plot via a printer in order to have the spectrum with all its acquisition parameters printed on paper.

IJSER © 2018
http://www.ijser.org

3.2 PEDRI System

The PEDRI system used is a low field imaging technique in order to bring the EPR frequency to 250MHz or less, which implies a low operational frequency and also requires EPR saturation in the sample of interest. The major components of the hardware system are as follows:

1. The magnet system
2. The NMR console.
3. RF coil assembly.

A basic block diagram of the instrument is as shown below in the following figure 3.7.

IJSER

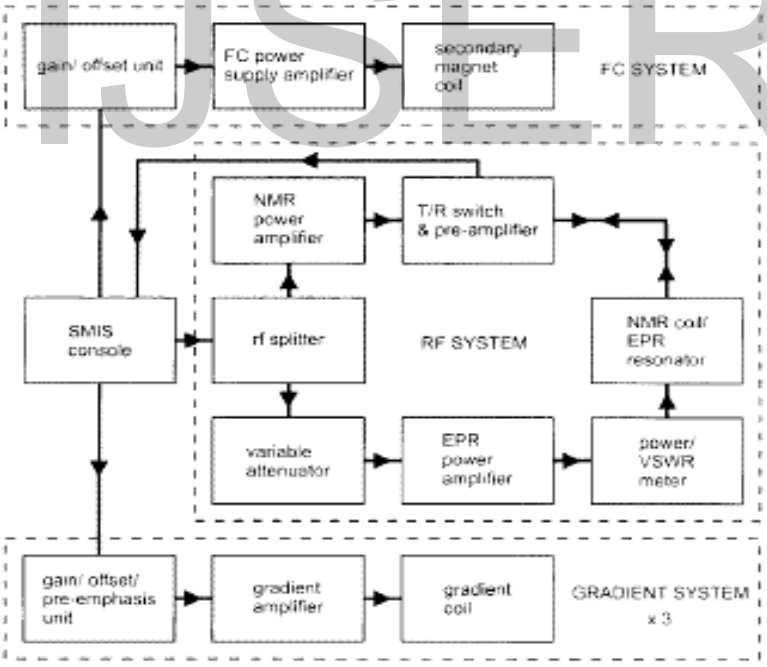

Figure3.7. Block diagram of the field-cycled PEDRI imager hardware. (Copied from reference [6])

IJSER © 2018
http://www.ijser.org

3.2.1 Magnet Structure

The PEDRI magnet system consists of the magnet with a cooling system, the stabilized power supply and a shielding mechanism. The whole body FC-PEDRI imager uses a whole body sized permanent magnet as the primary magnet and provides a vertical field of 59mT field required for NMR detection (Field effects Inc, Acton, MA, USA) as shown in the figure 3.6. Inside the bore of this permanent magnet is a resistive magnet, made from copper conductor in a saddle configuration, which is used for accomplishing field cycling by the field compensation method. The field from this secondary magnet can add to or subtract from the permanent magnet's field.[6] The offset field is generated by an internal resistive coil (Magnex Scientific, UK) driven by a power supply amplifier (Copley Controls, US). The gradient coils are built into the structure of the permanent magnet. The whole system has a bore of 52 cm inside the field cycling (FC) coil, the latter having an inductance of 68mH and a DC resistance of 0.66 ohm resulting in a time constant of 103 ms. The amplifier is able to ramp the magnetic field from 0 to 59 mT in 40ms. [6]

IJSER

The primary magnet is made from magnetized ferrite and weighs about 2500kg and has an internal bore of 0.65m. Its homogeneity is about 100ppm over a 30cm diameter spherical volume (DSV). The support structure of the magnet is made from composite materials, which are non-conducting and will not allow eddy currents to flow during field cycling. [6]

IJSER © 2018
http://www.ijser.org

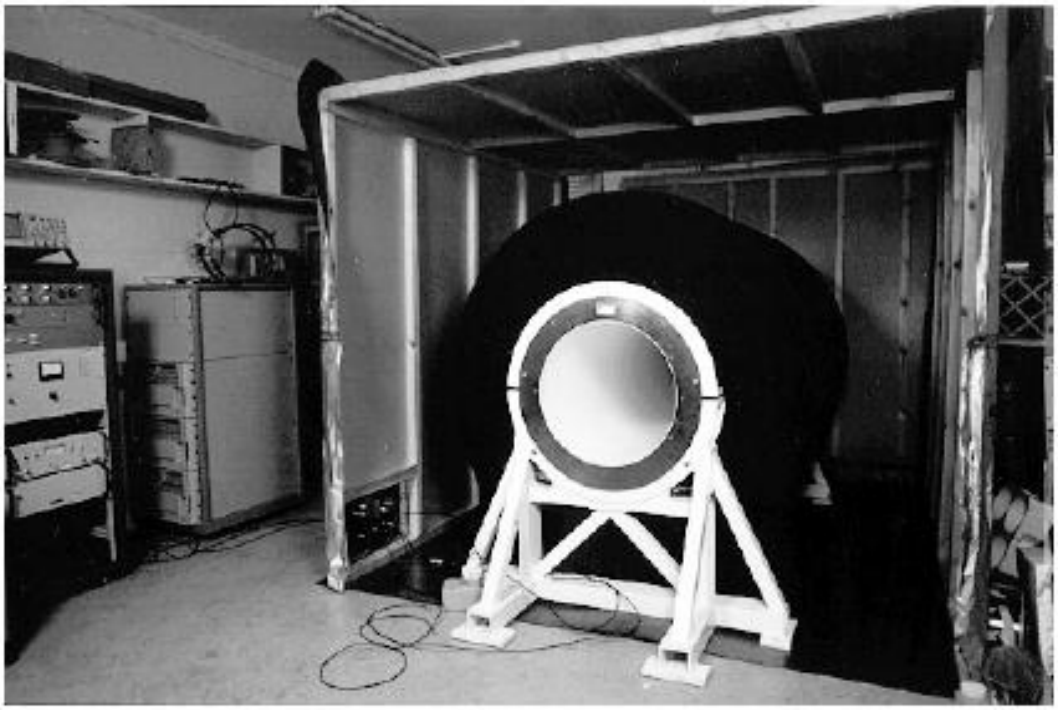

Fig3.8: Figure shows the whole-body FC-PEDRI imager. (Copied from reference [6])

IJSER

Figure 3.8 shows a photograph of the complete imager with the secondary magnet placed within the primary, the partially completed Farady screen is also seen. It is made from 40μm thick copper foil supported by a wooden structure. It is important that the screen conductor should not be very thick in order to minimize the eddy currents during field cycling.

The power supply amplifier (Copley Controls Inc., Westwood, MA, USA, model 265P), is powered by two 15kW DC power supplies (Electronic Measurements, Inc., NJ, USA, model ESS 330) operating in parallel. A 0.31F bank of capacitors connected across the 330V output of dc power supply provides the necessary current surges during rapid switching of the secondary coil current.[6]

Gradient hardware consists of bunched winding coils that can generate up to 10mT/m and are built into the structure of the primary magnet. They have a low resistance of approximately 55mΩ and a high efficiency (~ 0.13mT/m/A), which helps to minimize

IJSER © 2018
http://www.ijser.org

the thermal load on the magnet. Their inductances are 0.55mH (X and Y) and 0.67 mH (Z gradient coil). The coils are powered by gradient amplifiers (Crown International Inc., IN, USA, model Techron 7794), with one amplifier per channel. [6]

3.2.2 NMR Console

The PEDRI imager is controlled by a console SMIS Ltd, Guildford (UK) running on an integral IBM-compatible PC. which processes and displays the output signal. It supplies the EPR irradiation signal from an internal synthesiser. The console generates gradient and field cycling waveforms via 12-bit digital-to-analogue converters (DAC), along with TTL logic waveforms enabling or disabling external modules (RF amplifiers, field cycling amplifiers). Pulse programs are written in a C-like language and are compiled in the integral PC. [6]

IJSER

The console also includes a synthesized RF source (Programmed Test Sources Inc., MA, USA, model 310), which supplies the RF for the NMR excitation. NMR signals are demodulated within the console and sampled by 12-bit analogue to digital converters. A DSP card under control of the PC carries out the Fourier transform. [6]

3.2.3 Alderman Grant Resonator.

The FC-DNP spectroscopy and PEDRI experiments were carried out using a double-resonance coil assembly comprising an Alderman Grant Resonator (AGR) for ESR irradiation and a solenoid for NMR as shown in the figure 3.9. The AGR is basically a cylindrical coil assembly tuned to 121.5 MHz that generates a B_1 field perpendicular to its axis. The resonator (3.9(2)) is surrounded by a 20 cm diameter outer shield that

IJSER © 2018
http://www.ijser.org

is made of copper foil on a cylindrical Perspex frame. The resonator is driven initially via a coupling loop, connected to the signal source by coaxial cable (fig. 3.17 (1)).

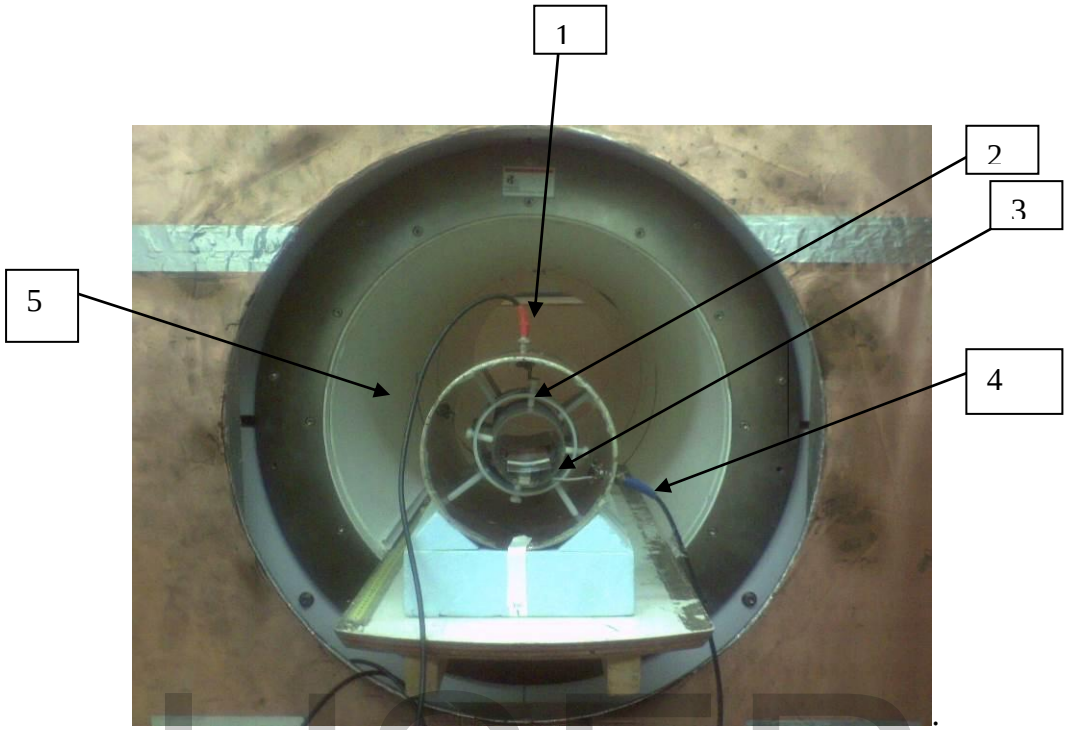

Figure3.9: Double Resonance Coil assembly AGR within the PEDRI imager (5). The EPR irradiation cable is connected at the top (1). The NMR solenoid connection is shown below (4).

IJSER

The NMR solenoid tuned to 2.494 MHz is placed inside the AGR coil (3.9(3)) and irradiation is provided through the cable shown in the figure (3.9(4)).

3.2.3.1 The NMR Solenoid

A continuous solenoid (length 7 cm, diameter 7.5 cm) was used for NMR transmit/ receive. The length of the coil was longer than the optimum value (5.25 cm) to improve the RF field uniformity at the expense of some loss in sensitivity. It is composed of 16 loops of a 3mm insulated copper wire mounted on a Perspex tube, leaving a solenoid axial length of 10 cm. This gives improved sensitivity at the expense of RF field uniformity. The two extremes of the solenoid are connected to a

IJSER © 2018
http://www.ijser.org

variable capacitor that matches the resonance frequency at 2.494 MHz. A tuning/matching circuit allows the solenoid to be tuned to the ^{1}H frequency (2.494 MHz). The distance between the loops is 3mm.

3.2.3.2 The AGR Dimension.

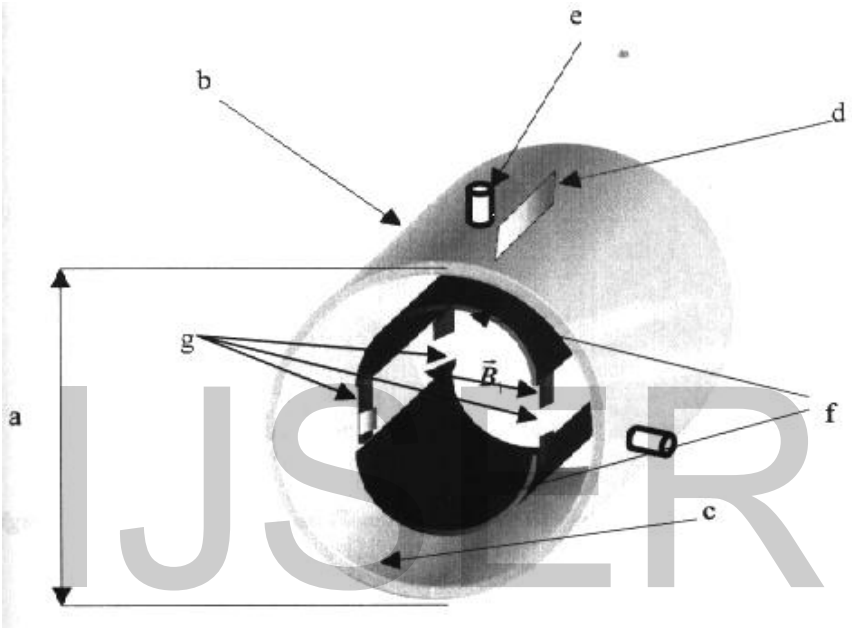

Fig 3.10: Alderman Grant Resonator with an outer shield that confines the magnetic field. This figure does not include the NMR receptor solenoid.

The AGR is surrounded by a 20 cm diameter outer cylinder (a) that is made of copper (b) surrounding a cylindrical Perspex (c) frame as explained before is shown in the above figure 3.10. The resonator is constructed from copper foil disposed on a PVC 11 cm diameter cylinder and tuned with ceramic capacitors placed symmetrically at each of the four gaps. The copper is arranged as two saddles (f) joined by four 15pF capacitors between two legs (g) form the resonator .The magnetic field B_1 is produced horizontally through the inside part of the resonator as shown in the figure 3.8. The

IJSER © 2018
http://www.ijser.org

plates (f) within the resonator are necessary to get an approximately sinusoidal current distribution to generate a homogeneous B_1. Inside the cavity left by the plates the NMR solenoid is placed. The resonator has a cylindrical arrangement: 9.0 cm in the axial dimension and 11.0 cm diameter. This part of the RF system allows a more uniform and horizontal EPR magnetic field inside the NMR solenoid.

IJSER

IJSER © 2018
http://www.ijser.org

CHAPTER 4 EXPERIMENTAL DETAILS.

As already mentioned a stable Nitroxide free radical was used in this project to compare the sensitivity of the ESR and PEDRI systems. The 2mM solution of the Nitroxide Tempol was prepared and was used as a standard solution for preparing the other less concentrated Tempol solutions. The later sections will give the details of the free radical used during the project and the procedures carried out while performing the experiment.

4.2 Nitroxide Tempol Structure

Free radicals are characterized by having an unpaired electron or vacancy in the outer orbital. The name is given as Nitroxide because the unpaired electron is localised on the N-O Bond. This unpaired electron is in close proximity to the nitrogen nucleus (^{14}N) as shown in the figure 4.1.

IJSER

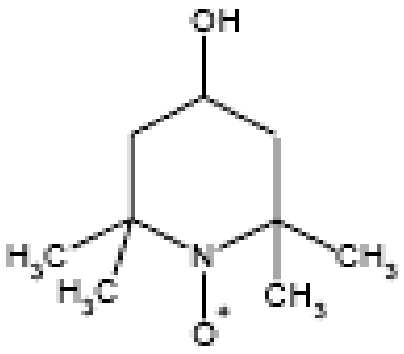

Fig 4.1: Structure of Nitroxide TEMPOL. (Copied from reference [5])

An ESR spectrum consists of a measurement of absorbed microwave power plotted against the external magnetic field. Sensitive spectrometers however use phase sensitive detection to enhance signal-to-noise ratios, which results the most real ESR spectra representing essentially the first derivative of power absorbed plotted against

IJSER © 2018
http://www.ijser.org

magnetic field. Hence a biphasic shape in the spectrum as seen in figure 4.2 represents the each line of resonance absorption. [2] This spectra not only indicates the presence of free radical but also gives the useful information on the chemical and physical nature of the paramagnetic species.[5] [7]

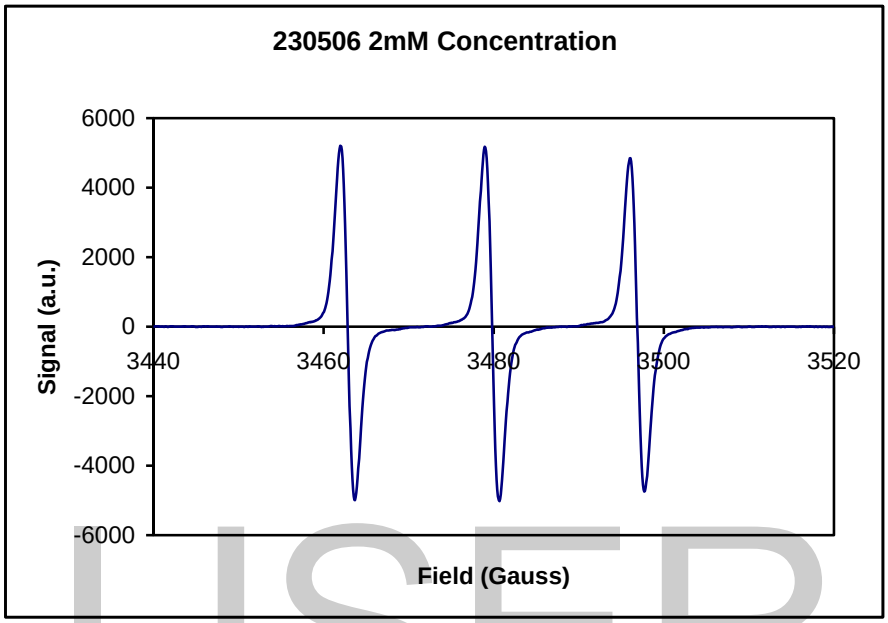

IJSER

Figure4.2: Typical ESR spectrum of 2mM Tempol solution obtained from Bruker ESR system.

4.3 Preparation of Samples

As mentioned earlier, one litre of 2mM Tempol Solution was used as a standard solution for preparing the other smaller concentrations of Tempol solution.

Since the formula weight of Nitroxide Tempol is 172.25, for preparing one litre of 1 molar solution needs 172.25 gm of Tempol. Hence 1 litre of 2 millimolar (2mM) needs 172.25 x 2x 10^{-3} g of Tempol.

The smaller concentration of Tempol i.e. 500ml of 1mM was prepared using the standard 2mM Tempol by doing the following calculation

$$\frac{1mM}{2mM} \text{ X } 500 = 250 \text{ ml of 2mM}$$

IJSER © 2018
http://www.ijser.org

So 250 ml of de-ionised water was added with 250 ml of 2mM Tempol solution to prepare 500 ml 1 mM Nitroxide Tempol solution. And the same procedure was carried out for preparing the rest of the smaller solutions from their preceding lower concentration Tempol solutions. For the experiments 13 different free radical concentration samples were prepared.

4.4 ESR Experiment.

In the ESR experiments the sample was held in a thin-walled quartz tube and the length of the sample in the tube is typically about 1cm as shown in figure 4.3(a). The sample container is termed a flat cell and the sample is held to lie in a part of the resonator where we get good EPR response as shown in figure 4.3(b). The flat part of the cell is the part inside the cavity and whose contents give the signal. The flat sample lies in the minimum E-field region, hence low losses. All the experiments were performed at room temperature.

IJSER

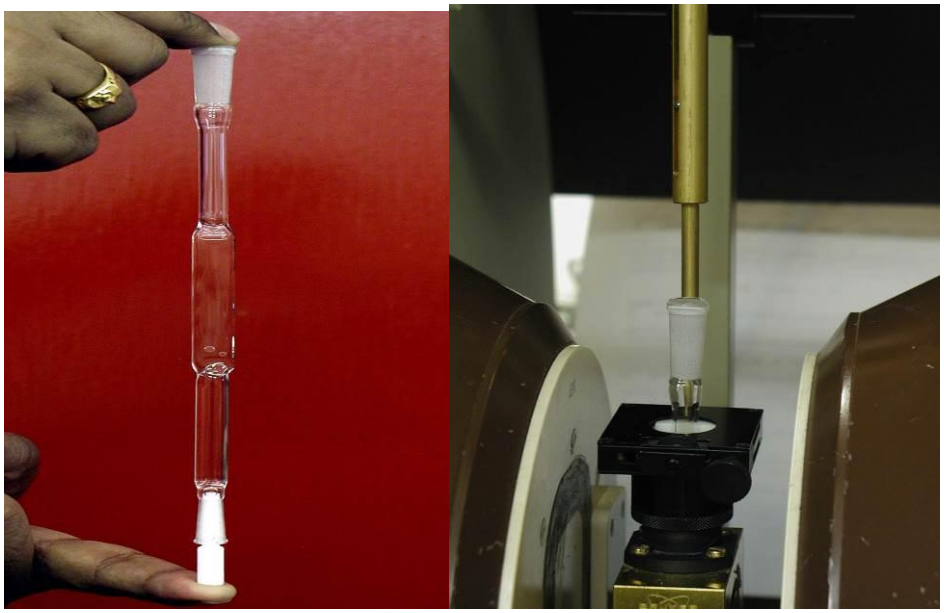

Fig4.3 (a): Flat cell- Quartz tube Fig (b): Picture showing sample in the cavity.

IJSER © 2018
http://www.ijser.org

After switching on the spectrometer, cooling system and magnet, signal channel, calibration had to be done for maximum sensitivity, minimum distortion and quantitative repeatable measurements. The initial signal channel parameters set or kept constant in the ESR system is as given below in the table 4.1.

Signal-Channel Parameters	**Values**
Modulation Frequency (kHz)	100.0
Resolution of field axis (Sets the number of data points per field sweep)	1024
Resulting Digitizer Resolution	14 bits
Resulting Sweep time.(seconds)	10.49

Table 4.1: Initial Parameters set before the ESR experiment.

IJSER

The next thing to be done is tuning of the microwave cavity in order to create an unperturbed wave pattern of the standing wave in the cavity. It also assures the maximum power transform to the sample. The tuning is done via the computer and manual fine tuning follows concerning frequency, phase and the bias current of the diode. For proper tuned signal we should see a dip in the display as shown in the figure 4.4. If not the microwave frequency is to be adjusted so that we see the dip in the middle of the display. The empty cavity will tune around 9.78 GHz. More operating details are found in the user's booklet for the ESR Bruker 300 system. [16]

IJSER © 2018
http://www.ijser.org

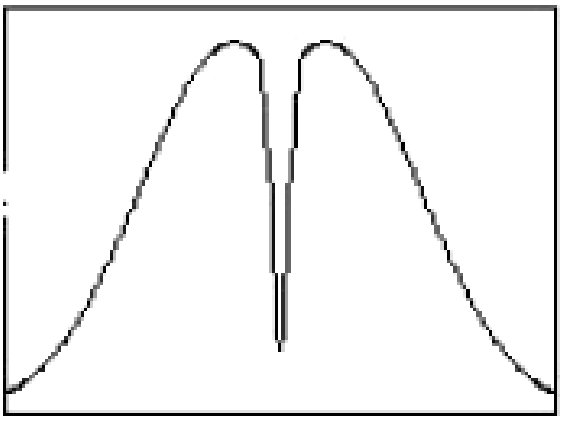

Fig: 4.4 Reflected signal (from the cavity) versus microwave frequency. The proper dip in the display assures the proper tuning of the cavity. (Copied from reference [16])

Magnetic field sweep is performed from 3440 gauss to 3520 gauss in order to find the spectrum. The centre field was 3480 gauss. The system resolution was standard 1024 points covering the sweep width. To get optimum and improved signal we should keep the gain as high as possible without distorting the spectrum. Signal strength is measured between peak to peak of the spectral line. [16] The entire spectrum acquired was stored as parametric file in the ESR bruker system. All parametric files were converted to DAT file which can be read by normal windows operating system to analyse the spectrum.

The important parameters to be adjusted and their significance in the ESR experiment are explained in tabulated form in the following table 4.2.

IJSER

IJSER © 2018
http://www.ijser.org

PARAMETERS	Function
Receiver Gain	Sets the amplification of the EPR signal. Increasing the Gain will increase the size of the signal, but if set too high the signal will be clipped off.
Modulation Amplitude	Increasing this parameter will increase the size of weak signals, but it also increases the distortion of the signal.
Time Constant	This parameter sets the time constant of the analogue filter i.e. this controls electronic filtering of noise. Making this value large will filter more noise, but it will also cause signal distortion if set too high. This should not be set higher than the conversion time.
Conversion Time	This is the time in milliseconds that is spent on converting each data each data point from its analogue value into its digital value. Higher conversion times give better results on noisy and weak signals, but will increase the scan time.

IJSER

Table 4.2: Parameters to be adjusted in ESR experiment. [16]

4.5 FC-DNP and PEDRI Experiment.

Small bottles and tubes are used to hold samples in FC-DNP spectroscopy and PEDRI imaging respectively which is shown in fig 4.5 (A) and fig 4.5 (B).

The shimming of the magnetic field is first carried out to make the magnetic field as homogeneous as possible and the next step was to note the offset frequency. The default NMR frequency value is corrected by adding the observed offset value. For example the offset observed was –1600. This value is added with the initial frequency of 2.494 MHz giving 2.4936MHz. Later the 90^0 RF pulse value of 90 μs is found by observing the highest signal.

IJSER © 2018
http://www.ijser.org

4.5.1 FC-DNP Spectroscopy Experiment

(A) *(B)*

Figure 4.5: (A) Bottles used to place samples in FC-DNP Spectroscopy experiment (B) Small tubes used in PEDRI imaging experiment.

IJSER

The tuning is fixed to the right frequencies: 2.495 MHz approximately for the NMR frequency and about 121 MHz for the EPR frequency with the help of a network analyser. Once the capacitors are adjusted to minimize reflections (reflection of EPR power that arrives to the AGR and reflection of the signal that goes from the NMR solenoid with the junction with the coaxial cable), the next step was to ensure the sample within the resonator was set in the middle of the PEDRI unit to coincide with the centre of the magnet as shown in figure 4.6. After that the EPR cable is reconnected to the power meter. The attenuation control on the console unit was used to vary the power output to the EPR coil.

IJSER © 2018
http://www.ijser.org

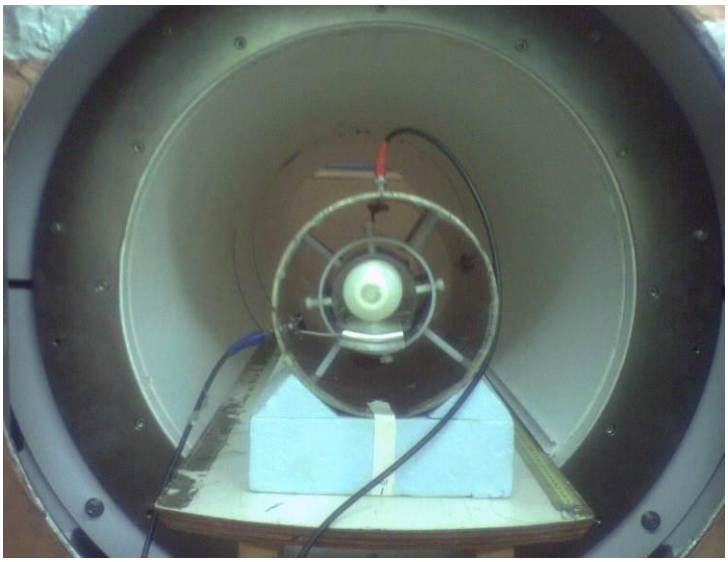

Figure 4.6: Sample placed in A.G.R Coil during FC-DNP spectroscopy experiment.

Parameters	**Value**
NMR frequency	2.4936 MHz
90^0 degree pulse duration	80 µs
Tuned and matched ESR frequency	123.268 MHz
Power of ESR Irradiation	20 watts
Attenuation of ESR irradiation signal	25 dB
ESR Irradiation Time	500 ms

IJSER

Table 4.3: Parameters used for FC-DNP experiment.

Once the EPR irradiation frequency is chosen the next important step in PEDRI is the determination of the B_0^E field at which the EPR irradiation can be carried out and at which the Overhauser enhancement is maximum. A typical FC-DNP spectrum obtained for 2mM Concentration is shown in the following figure 4.7:

IJSER © 2018
http://www.ijser.org

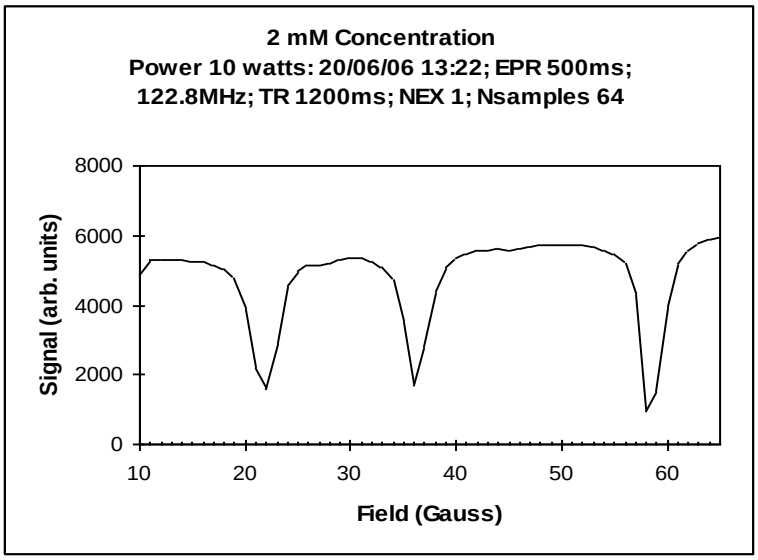

Figure 4.7: FC-DNP Spectrum of a 2mM Tempol with an EPR radiation frequency of 122.746MHz.The resolution of this spectrum is 1 Gauss.

The spectrum consists of three dips where the NMR signal amplitude is most affected by the Overhauser effect. According to quantum theory at low magnetic fields σ transitions are induced in regions where the B_1 field produced by the EPR coil is parallel to the main field. The two less prominent dips observed in the figure 4.8 at 28G and 44G indicate the presence of σ transitions.

IJSER

The Overhauser effect produces a negative enhancement of the proton magnetisation and therefore the peaks are inverted. The third peak at 58 Gauss i.e. B_0^E was found and the experiment was carried around this value with higher resolution for the same sample with the same parameters set and the spectra obtained is shown in the figure 4.8. All spectrum data acquired were analysed in Windows MS-Excel.

IJSER © 2018
http://www.ijser.org

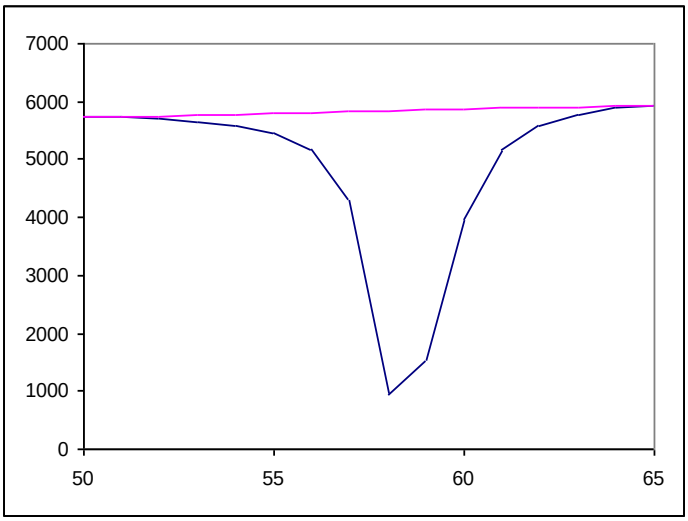

Fig: 4.8 FC-DNP Spectrum of a 2mM Tempol with an EPR radiation frequency of 122.746MHz. The pink line gives the initial signal before irradiation. It is used to calculate the total enhanced signal.

IJSER

4.6.2 PEDRI Experiment.

In PEDRI imaging experiments the steps are repeated as in FC-DNP spectroscopy but the spin warp imaging pulse sequence is used in addition to collect images typically with 64x64 pixels. The FC-PEDRI pulse sequence parameters B_0^E and the EPR irradiation frequency are set to the values determined as explained in the earlier FC-DNP Spectroscopy experiment.

The experiment was performed by using four different free radical concentration samples along with a copper sulphate solution ($CuSO_4$) which does not contain free radical. The figure 4.9 shows the configuration of the samples used to perform PEDRI imaging and figure 4.10 shows the samples placed in the PEDRI imager unit for performing the experiment.

IJSER © 2018
http://www.ijser.org

Parameters	**Value**
TR (Repetition time)	1500ms
Echo time (TE)	26ms
Evolution Magnetic field	59.0 Gauss

Table4.4: Parameters Setup for PEDRI Imaging pulse sequence

The FC-PEDRI pulse sequence is an interleaved pulse sequence with alternate NMR excitations preceded by a period of EPR irradiation. This results in two data sets namely the with-EPR image data and the without-EPR image data. The raw NMR data collected is then processed using software that generates a file which when Fourier transformed results in three different image files namely the NMR image with EPR irradiation and the third being the difference of these two images.

IJSER

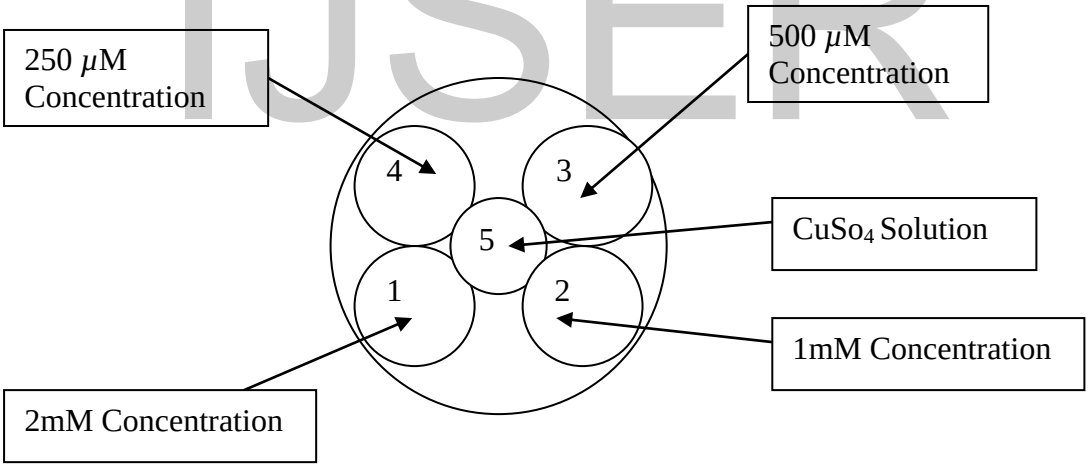

Figure 4.9: The above picture shows the configuration of the samples used for PEDRI Imaging.

The difference image shows non-zero intensity only in regions containing the free radical of interest as seen in figure 4.11(b).

IJSER © 2018
http://www.ijser.org

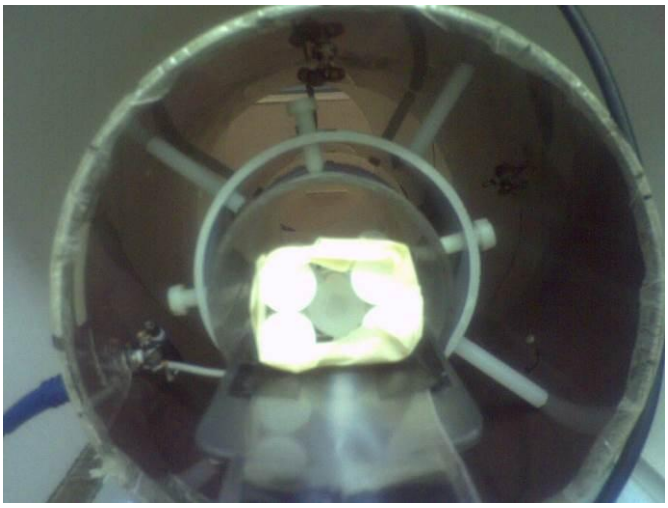

Figure 4.10: Samples placed in the AGR Coil with the orientation shown in the above figure 4.9 during PEDRI Imaging.

The Fourier transformed data was then displayed using the image display program as shown in the figure 4.11(a) and the difference image obtained by performing the experiment for the samples in the configuration shown in the fig 4.9 is shown in fig 4.11(b).

IJSER

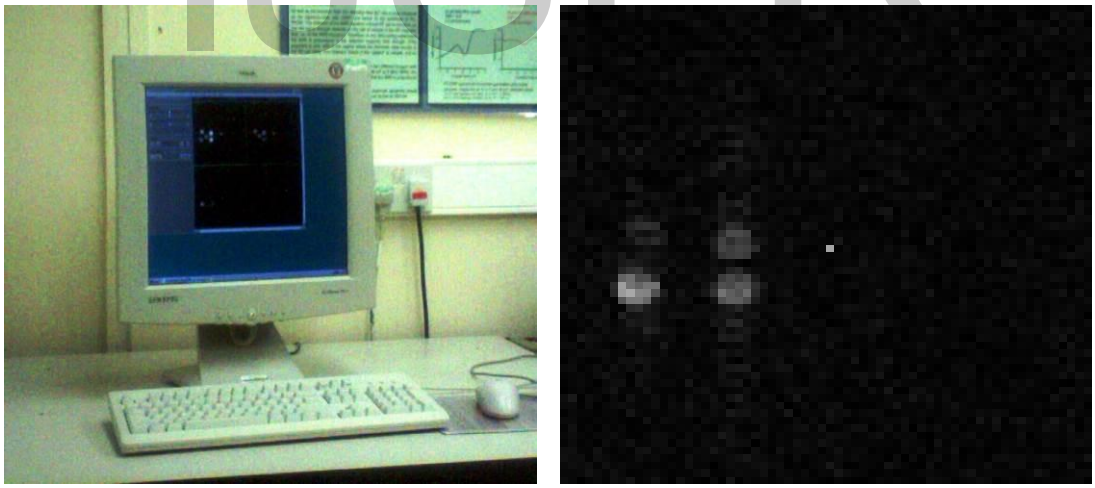

Figure 4.11: (a) PEDRI Image display. (b) The Difference image showing only the presence free radicals with different concentrations obtained with scaling factor of 0.08 and EPR irradiated with 123.006MHz using PEDRI system.

IJSER © 2018
http://www.ijser.org

CHAPTER 5. RESULTS AND DISCUSSION

5.1 ESR Results

As explained in section 4.5, signal channel calibration should be done and initial parameters mentioned in table 4.1 should be kept constant before the experiment is carried out. The main parameters which are varied during ESR experiment to analyse the sensitivity of the ESR Bruker 300 system are as follows:

1) Attenuation
2) Time Constant
3) Conversion Time
4) Modulation Amplitude
5) Gain

Each parameter have significant effect on detecting the ESR spectra and varying these parameters appropriately enables to improve the sensitivity of the ESR system. The next sections explain the result obtained from the experiment and outlines the importance of the above parameters mentioned.

IJSER

5.1.1 Effect of Attenuation on SNR.

Signal-to-noise ratio is the ratio between a signal (meaningful information) and the background noise. Attenuation is a general term that usually refers to any reduction in the strength of a signal. In our experiment Attenuation is used in controlling the transmission of the microwave power and to analyse the way it affects the SNR of the ESR spectra obtained. The table 5.1 gives the details of the parameters kept constant.

IJSER © 2018
http://www.ijser.org

Parameters	Values
MA (Gauss)	0.8
TC (ms)	20
CT (ms)	40
Gain	6.30E+02

Table 5.1 Initial parameters kept constant

Using these parameters, the attenuation is increased for every signal acquisition and the resulting SNR values are used to plot the graph of SNR vs. Attenuation as shown in figure 5.1 to analyse the effect of attenuation.

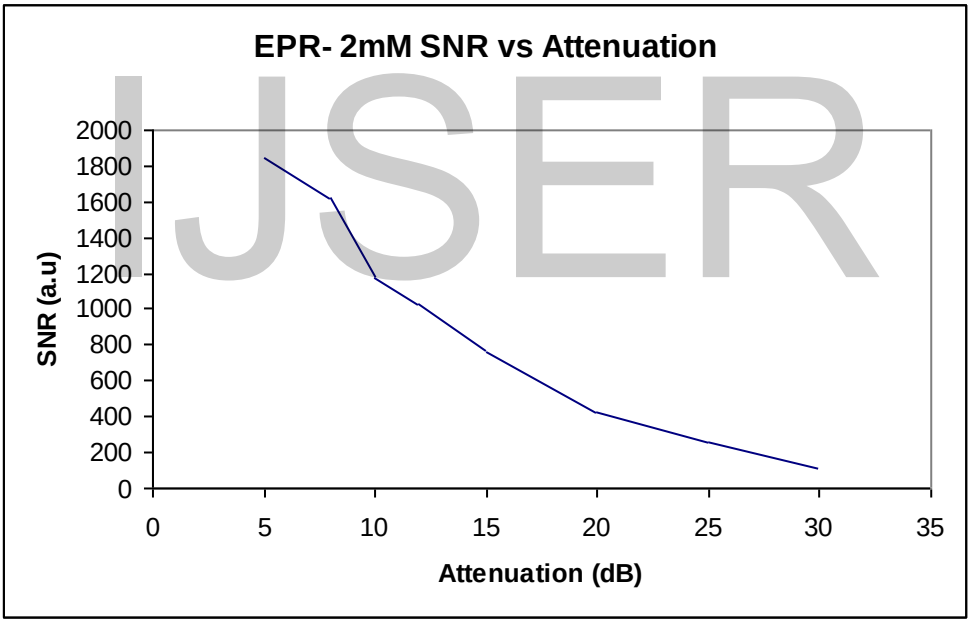

IJSER

Fig5.1: Figure showing the effect of Attenuation on SNR for the 2mM Tempol solution.

As the attenuation is increased the microwave power transferred to the sample is reduced and hence we get less ESR signal from the sample. So when attenuation is kept low the sensitivity of the system increases as seen from the figure 5.1. The ESR

IJSER © 2018
http://www.ijser.org

phenomenon is greatly observed when the power is increased as shown in figure 5.2, but doing that we are depositing more power in the sample which is not desired when experimental is carried out for in-vivo samples. Also for the higher power levels the sample shows saturation that is explained in the next paragraph.

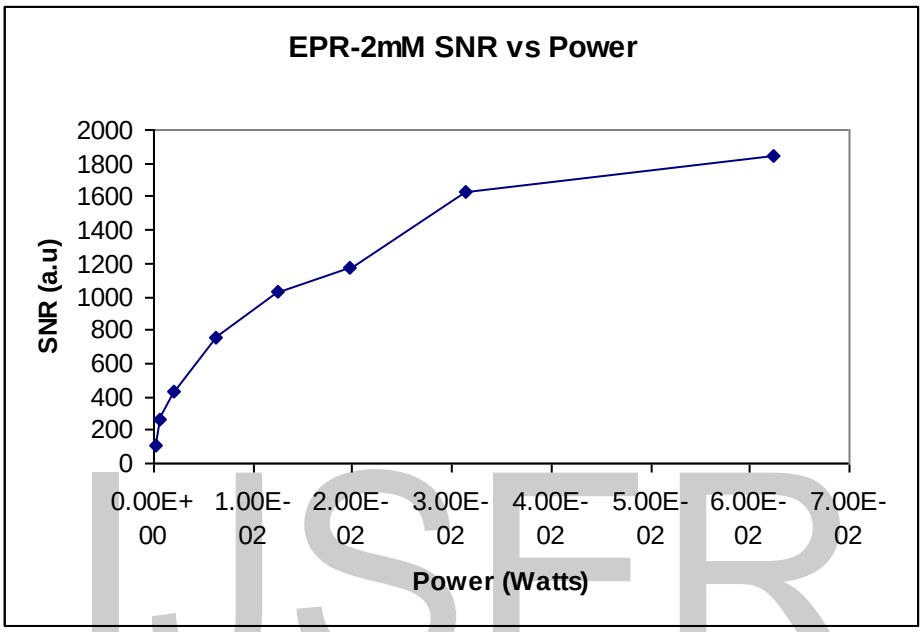

IJSER

Fig5.2: Figure showing the effect of Power on SNR for the 2mM Tempol solution.

An excessive power setting, P, can cause a decrease in, or elimination of, the ESR signal due to sample saturation. This can be seen especially in samples having relatively long relaxation times (with sharp resonance lines). Signal intensity is proportional to $\sqrt{P}$ in the region where saturation does not occur. The linear region of plot of I vs. $\sqrt{P}$ indicates suitable power levels i.e. the sample does not saturate and we get the proper signal as shown in the figure 5.3. [16]

IJSER © 2018
http://www.ijser.org

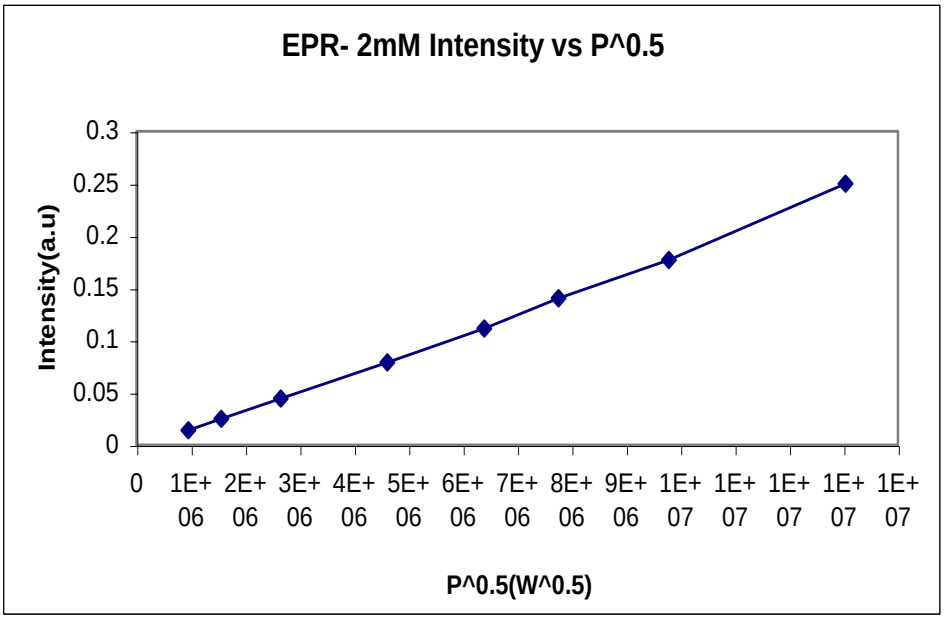

Fig5.3: Figure showing the effect of Power on Intensity for the 2mM Tempol solution.

IJSER

5.1.2 Effect of Modulation Amplitude on SNR.

The Modulation Amplitude (MA) parameter is used to increase the size of the weak signals thereby improving the SNR of the spectrum obtained as seen in figure 5.4. The table 5.2 gives the detail of initial parameters kept constant for performing the experiment. But this may be seen until some point. Excessive values, those greater than the line width will broaden and distort the resonance line.

Parameters Kept Constant	
TC	20ms
Attenuation	10dB
CT	40 ms
Gain	6.30E+02

Table 5.2: Initial parameters kept constant

IJSER © 2018
http://www.ijser.org

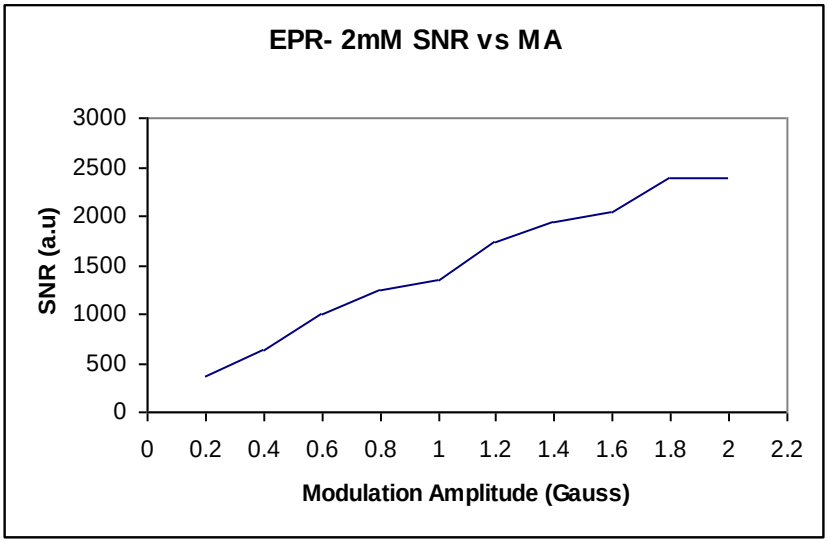

Fig 5.4: Figure showing effect of Modulation Amplitude on SNR.

As we see from the following figure 5.5, at higher modulation amplitude values the measured line width is gradually increased and is not suitable for ESR spectroscopy as it will broaden the line and distort the resonance. So for a non-distorted line shape, the MA value should be chosen in between the limits as stated in the following expression.

IJSER

$$\frac{1}{10}\Delta B_{pp} \leq MA \leq \frac{1}{2}\Delta B_{pp} \ldots\ldots\ldots\ldots\ldots 5.1$$

Where ΔB_{pp} is the distance of peak to peak in terms of magnetic field as shown in the following figure 5.5.

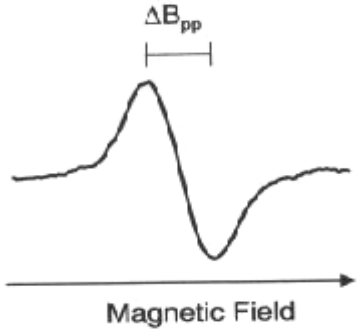

Fig. 5.5: The distance of peak to peak in terms of magnetic field. (Copied from reference [1])

IJSER © 2018
http://www.ijser.org

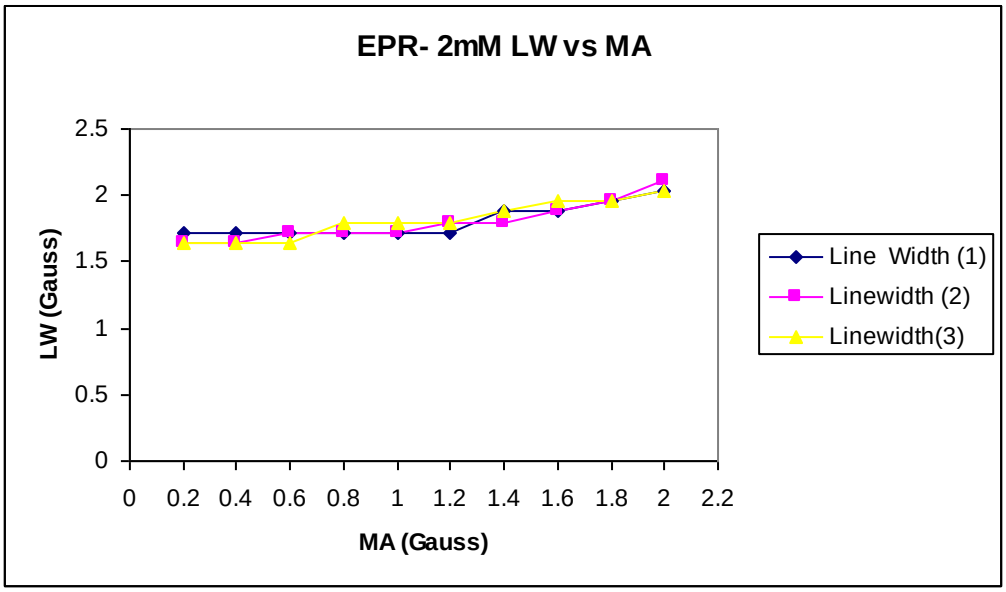

Fig 5.6: Figure showing effect of Modulation Amplitude on Line Width.

5.1.3 Effect of Time Constant on SNR.

The Time Constant (TC) parameter controls electronic filtering of noise. Making this value large will filter more noise and SNR is improved as observed from the figure 5.7, but it will also cause signal distortion if set too high i.e. the minimum and maximum peak value ratio does not show unity values i.e. the asymmetry of maximum and minimum peaks will occur as shown in the figure 5.8. The equation for Asymmetry is given in the following equation 5.2.

$$\text{Asymmetry} = \frac{Maximum}{|Minumum|} \quad \ldots\ldots 5.2$$

The table 5.3 gives the detail of parameters kept constant for this experiment.

Parameters Kept Constant	Values
Attenuation	10db
CT	40 ms
MA	0.8G
Gain	6.30E+02

Table 5.3: Initial parameters kept constant

IJSER

IJSER © 2018
http://www.ijser.org

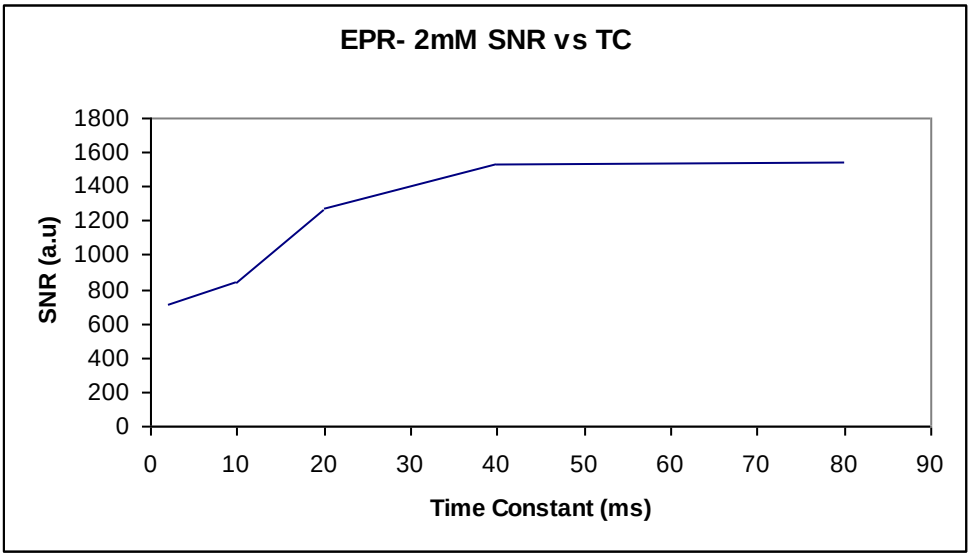

Fig 5.7: Figure showing effect of TC on SNR.

The Noise (N) of the signal is proportional to the TC (τ) i.e. $N \alpha \tau^{-1}$. As explained earlier if the time constant is too large, the danger is that the signal itself can be filtered out. For undistorted lines shapes, scan time should be kept ten times or more than that of TC i.e. scan time $\geq 10\ \tau$, where scan time is the time required to scan through the narrowest resonance line.

IJSER

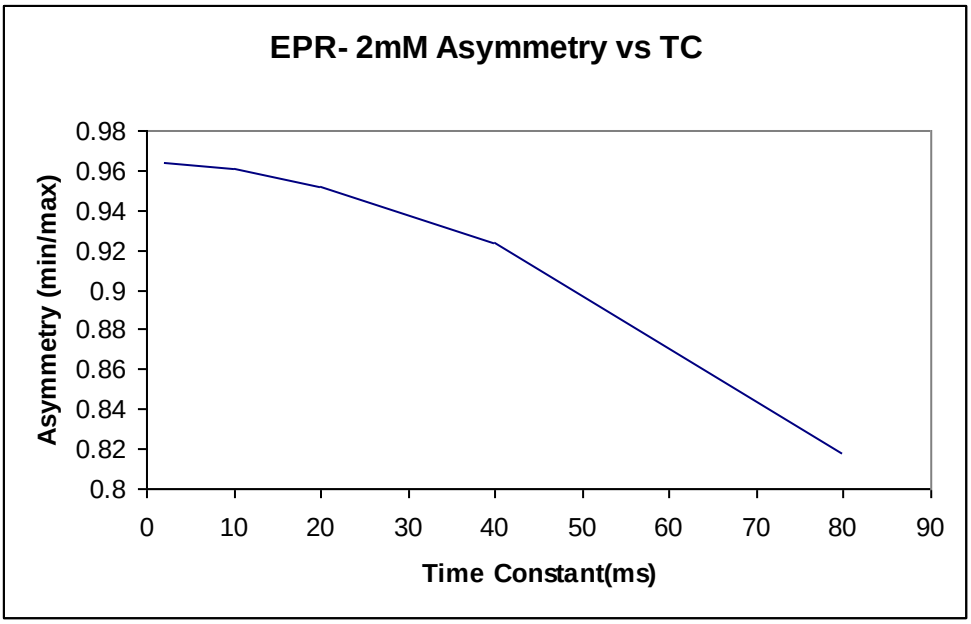

IJSER © 2018
http://www.ijser.org

Fig 5.8: Figure showing effect of TC on signal.

The value of Time Constant should not be set higher than the conversion time, because there will be no improvement in SNR as seen from the figure 5.7. Instead asymmetries of positive and negative peaks are observed i.e. distortion of the signal, which is clearly seen from the graph in the figure 5.8.

5.1.4 Effect of Gain on SNR.

Gain used to be adjusted to get optimum signal which covers the dynamic range of the ADC. The ADC voltage range is covered by 14 bits. High gain results in clipping of the signal due to overload effect. Gain should be adjusted to get sharp peak signals with good SNR. Lowering the gain also reduces SNR and signal is distorted and also does not use the full dynamic range of ADC. The table 5.4gives the detail of parameters kept constant for this experiment.

IJSER

Parameters Kept Constant	**Values**
MA (G)	2
CT (ms)	10.24
TC (ms)	40
Attenuation(dB)	10

Table 5.4: Initial parameters kept constant

IJSER © 2018
http://www.ijser.org

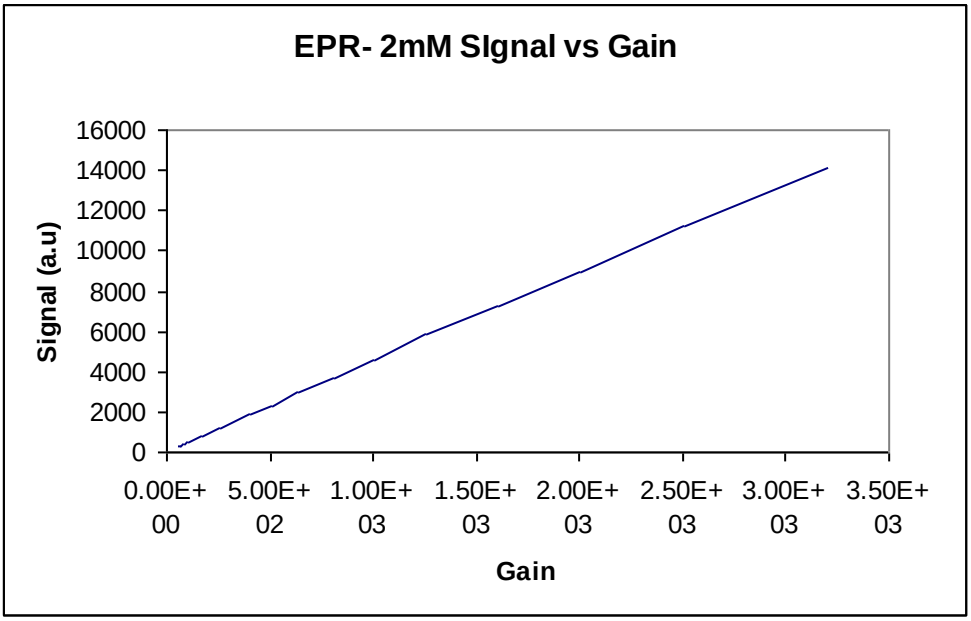

Fig 5.9: Figure showing effect of Gain on signal.

The best signal-to-noise ratio (S/N) is obtained with an optimal receiver gain setting and from figure 5.9 and 5.10 we can see that increasing the gain optimally gives better signal with high SNR. As we see from figure 5.8, when the gain was increased from 1000 to 3000 the signal was increased from 4000 to 14000 i.e. almost three and half times the signal was increased.

IJSER

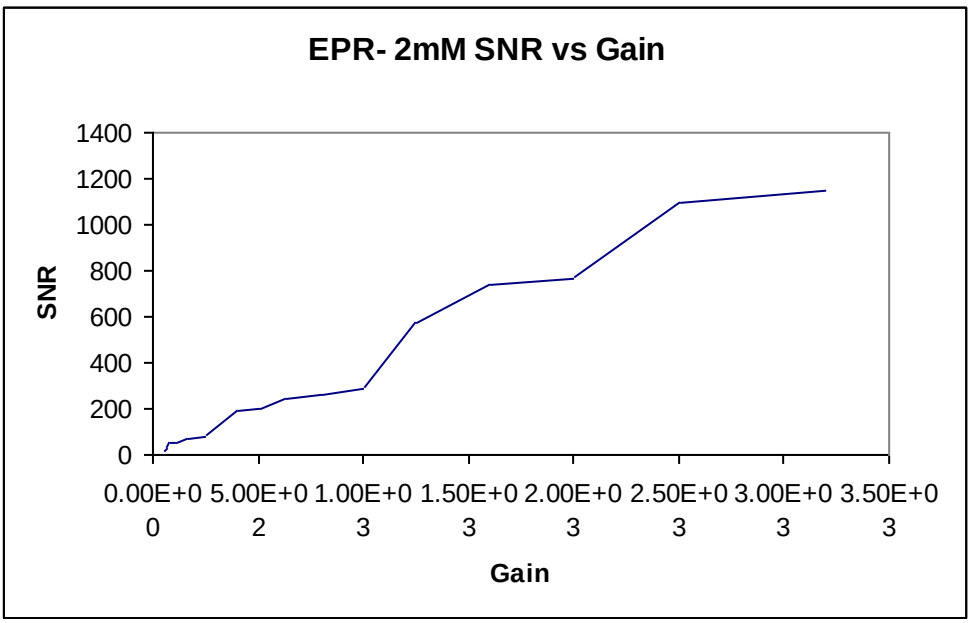

Fig 5.10: Figure showing effect of Gain on SNR.

IJSER © 2018
http://www.ijser.org

5.1.5 Effect of TC and CT on ESR Sensitivity.

In this experiment the TC and CT values are varied suitably as given in the table 5.5 for the lowest concentration of free radical i.e. 0.01 µM Tempol solution to improve the sensitivity of ESR system.

Time constant (ms)	Conversion Time (ms)	Parameters Kept Constant	Values
40	10.24	MA (G)	2
81	20	Attenuation (dB)	10
163	40	Gain	1.60E+06
327	81		

Table 5.5: The table shows the parameters TC and CT varied keeping other parameters constant.

IJSER

The signal level is increased to 13000 approximately at higher TC and CT values compared to the lower TC and CT values where the signal was low i.e. 2500 approximately. Hence the signal level was increased 5 times more than the signal measured at lower TC and CT values, which can be clearly seen from the figure 5.11.

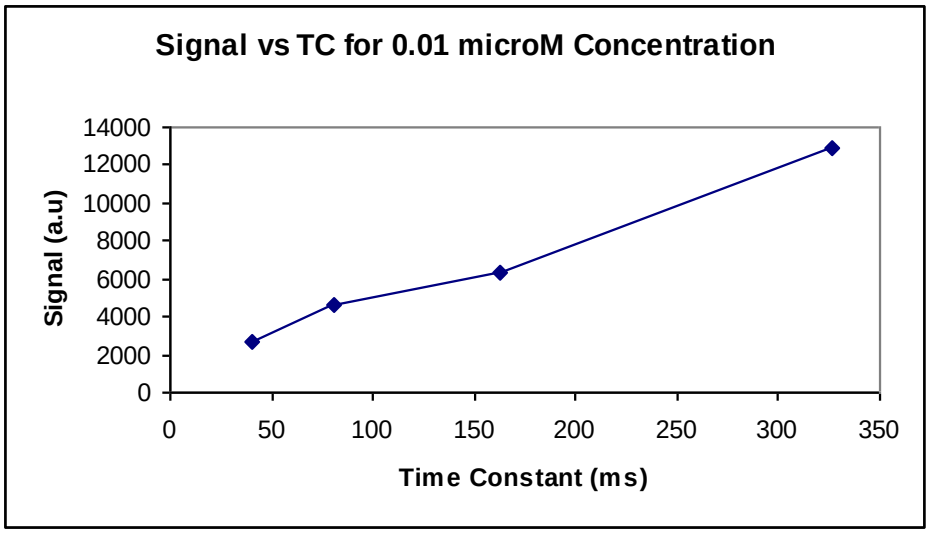

Fig 5.11: Figure showing effect of TC on Signal.

IJSER © 2018
http://www.ijser.org

Even the SNR was better at higher TC and CT values compared to lower TC and CT values, which can be seen from the following figure 5.12.

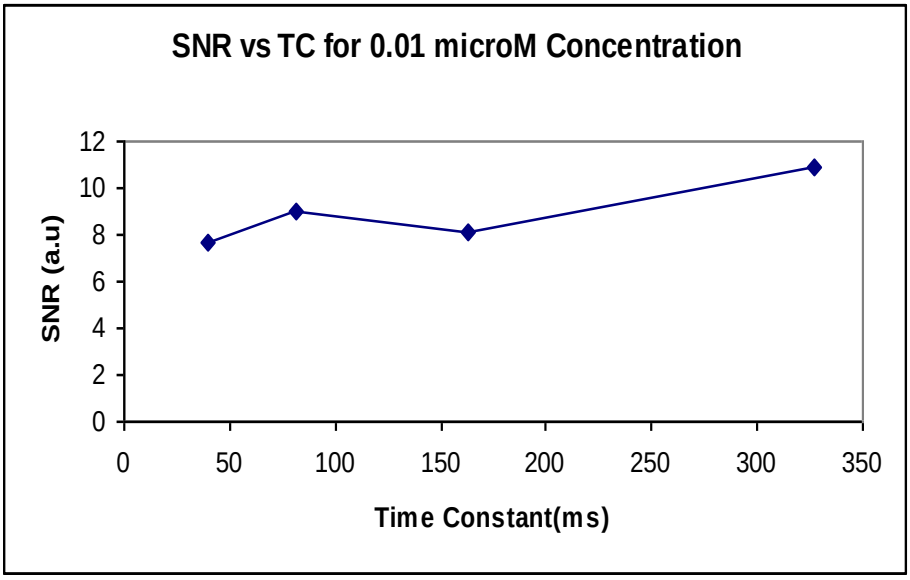

Fig 5.12: Figure showing effect of TC on SNR.

IJSER

As explained in table 4.2, higher conversion times give better results on noisy and weak signals, but will increase the scan time and also the threat of signal distortion for higher TC values as explained in section 5.1.3. So for lower concentrations we have to compromise the things mentioned before for acquiring good signal. Hence there is risk of losing accurate information for the given sample.

5.1.6 Consistency Check Of The ESR System

The consistent performance of any system is very important in determining the true ESR spectra and concluding the sensitivity of the system. The consistency check was performed by using the 2mM Tempol concentration sample. The sample was placed in the microwave cavity and the tuning and matching procedure was carried out, followed by the acquisition of spectra. The sample was then removed from the cavity, then replaced, and the procedure was carried out again. The table 5.4gives the detail

IJSER © 2018
http://www.ijser.org

of parameters kept constant for this experiment. In total 10 spectra were obtained and the values obtained are analysed as shown in the figure 5.13.

Parameters are kept constant	**Values**
Attenuation	10db
MA	2G
TC	40ms
CT	10ms

Table 5.6: The table shows the initial parameters kept constant.

Ideally the system should show the same measured SNR values, since the sample and parameters used are identical for every test.

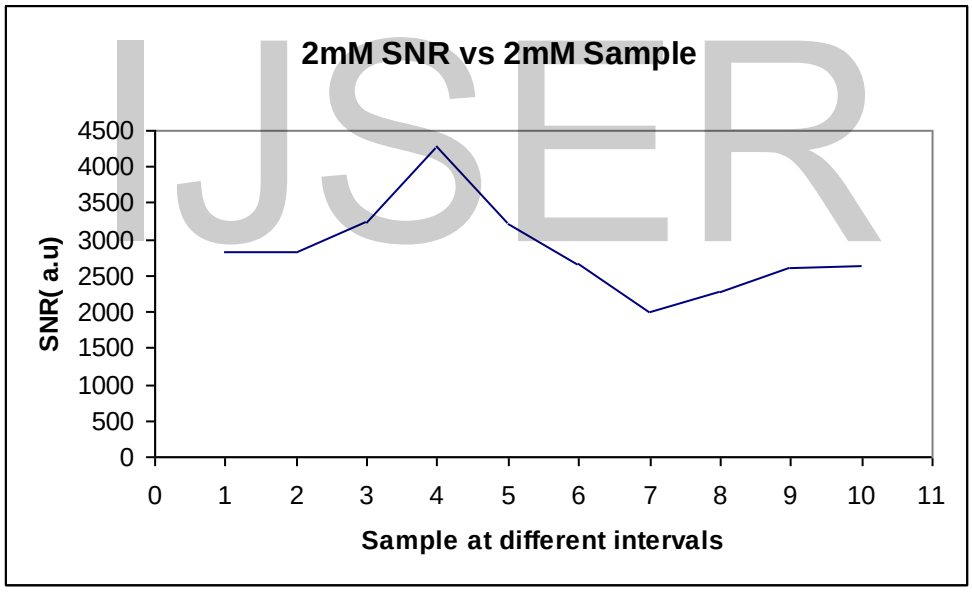

Fig 5.13: Figure showing inconsistency of the Bruker ESR system.

The figure 5.13 clearly shows the inconsistency of the ESR Bruker 300 system. Hence the results obtained from the experiments are not entirely the true values, because of the inconsistent nature of the ESR system. Even the operator errors are also taken into

IJSER © 2018
http://www.ijser.org

account as he may not place and tune the sample properly in the cavity. Hence the errors may be due to the system as well as from the operator.

5.1.7 Analysis of Sensitivity.

The measured signal level is increased at higher concentrations of free radical. The signal level decreases with lower free radical concentrations and the measured signal values for different concentrations are plotted in the figure 5.14. The table 5.7 gives the detail of parameters kept constant while performing the experiment for all different concentrations.

Parameters Constant	**Values**
MA (G)	2
CT (ms)	10.24
TC (ms)	40
Att. (dB)	10

Table 5.7: The table shows the initial parameters kept constant.

IJSER

The gain was set to 1000 for detecting 1 mM concentration and later the gain was increased for the lower concentration samples. The intensity values measured and calculated for all the samples for compensating the gain factor of 1000 as set for 1mM. The measured signal intensity at 1mM concentration was 13943 and 2733 for 0.01 μM concentration. The signal had dropped five times down for the 0.01 μM concentration compared to the signal level measured for 1 mM concentration. But the expected SNR for the 0.01 μM concentration should drop down by 100000 times compared to the value measured for 1 mM concentration.

Hence it is clear from the figure 5.14 that the sensitivity is higher at higher concentrations of free radical and the sensitivity goes down for lower concentrations. The error bars in the figure 5.14 shows the variation in the measured signal values due to the system inconsistency and operator error as explained in section 5.1.6. The

IJSER © 2018
http://www.ijser.org

signal variation observed is higher at higher concentration, may be due to the higher sensitivity for higher concentrations and vice-versa for lower concentrations. All the signal values measured are compensated for the gain value of 1000.

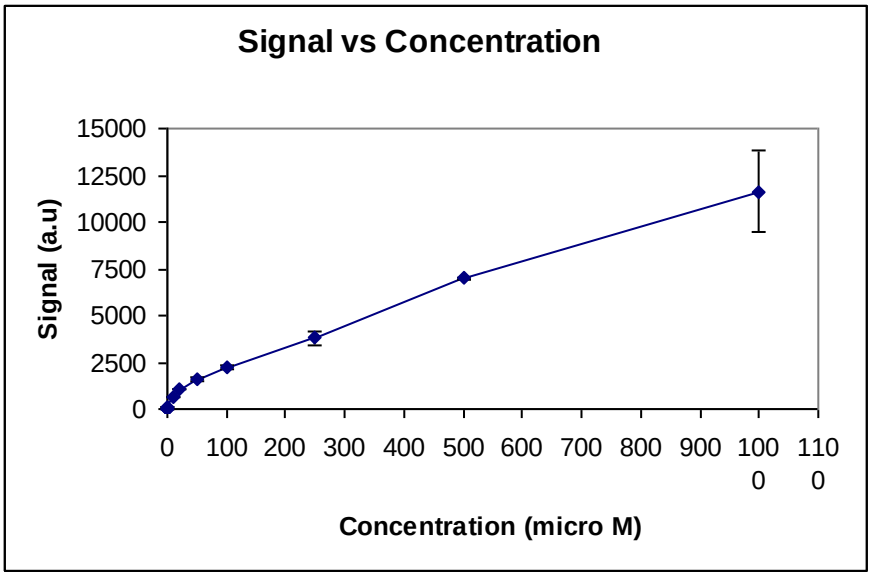

Fig 5.14: SNR versus different concentrations of TEMPOL solution samples.

IJSER

It was expected that the SNR would drop for the lower concentrations, but from the figure 5.15 the system showed unexpected behaviour. And again it may be the cause of the systems inconsistency behaviour and as well as the operator error.

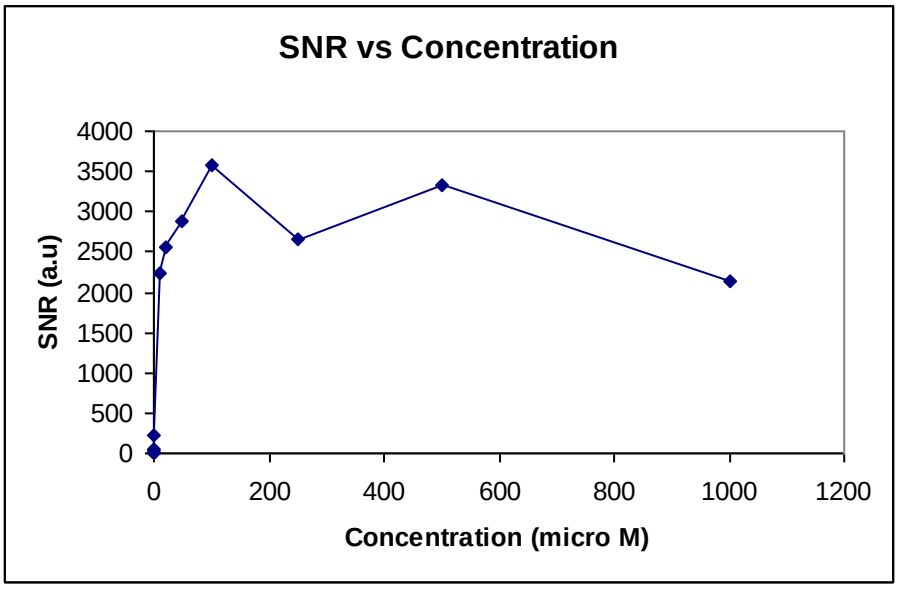

Fig 5.15: Figure showing the sensitivity of the Bruker ESR system.

IJSER © 2018
http://www.ijser.org

5.2 FC-DNP Results

In the FC-DNP spectroscopy the spectra obtained for the free radical sample as shown in the figure 5.16 is used to evaluate the parameters i.e. Initial Signal (S_0), Signal(S) , Enhancement factor (E) and Overhauser factor (A).The S_o is the signal when ESR irradiation is OFF and the S is the signal acquired when the sample is irradiated i.e. ESR is ON. The figure 5.16 shows the S_0 and the S i.e Initial signal and Measured signal.

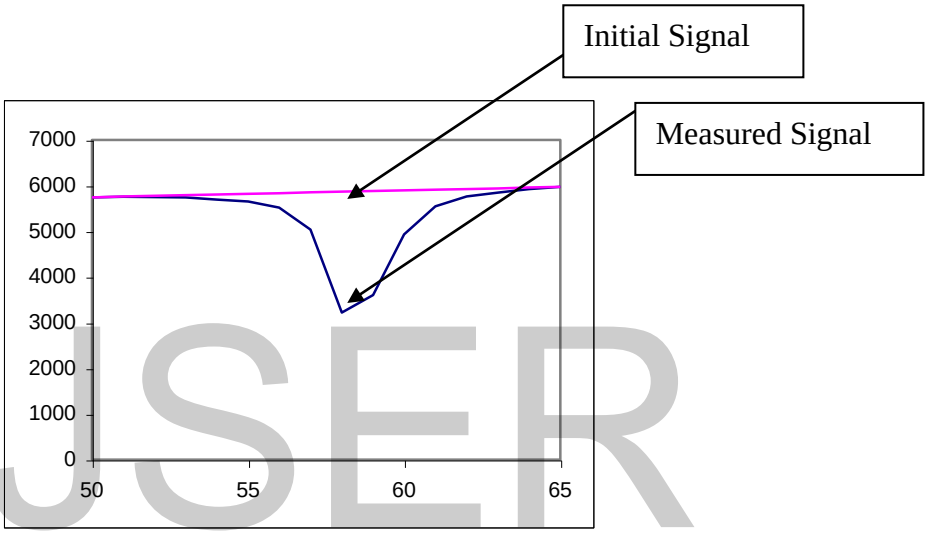

IJSER

Fig: 5.16 A typical FC-DNP spectra

The noise (N) is the standard deviation of the region of the spectrum away from the spectral line. The Overhauser factor (A) is calculated by the following equation 5.3:

$$1\text{-}E = A \quad \ldots\ldots 5.3.$$

Where E is the Enhancement factor, which is calculated as given in the following equation 5.4:

$$E = \frac{S}{S_0} \quad \ldots\ldots\ldots 5.4$$

IJSER © 2018
http://www.ijser.org

5.2.1 Effect of ESR Irradiation Power.

Attenuation(dB)	Power (watts)	SNR	Overhauser Factor (A)
40	1	7	0.03
32	5	37	0.19
28	10	123	0.34
26	15	168	0.48
25	20	725	0.67
23	30	1245	0.76

Table 5.8: The above table shows the data for 1mM free radical sample while ESR irradiation time of 500ms was kept constant.

As the Power was increased the Overhauser effect is increased also the SNR of the spectra was also increased which is shown in the figure 5.17 and figure 5.18 respectively. This effect was seen for all the rest of the samples on which the experiment was performed. The table 5.8 gives the parameters varied and also the results obtained i.e. SNR and the Overhauser factor.

IJSER

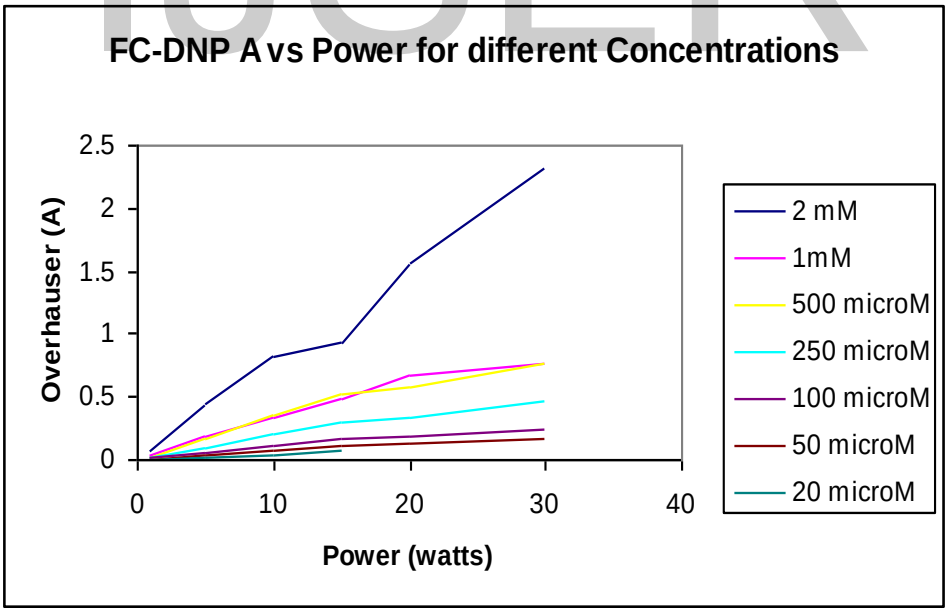

Fig 5.17: Overhauser Effect versus Power for different concentrations of TEMPOL solutions while ESR irradiation time of 500ms was kept constant.

IJSER © 2018
http://www.ijser.org

The Overhauser effect is reduced for the lower free radical concentration samples, which can be clearly seen from the above figure 5.15. This indicates that the Overhauser effect is proportional to the amount of the free radical concentration and also the Irradiation power . The lowest concentration which was clearly detected or had shown Overhauser effect by using the PEDRI system was 20 µM free radical concentration.

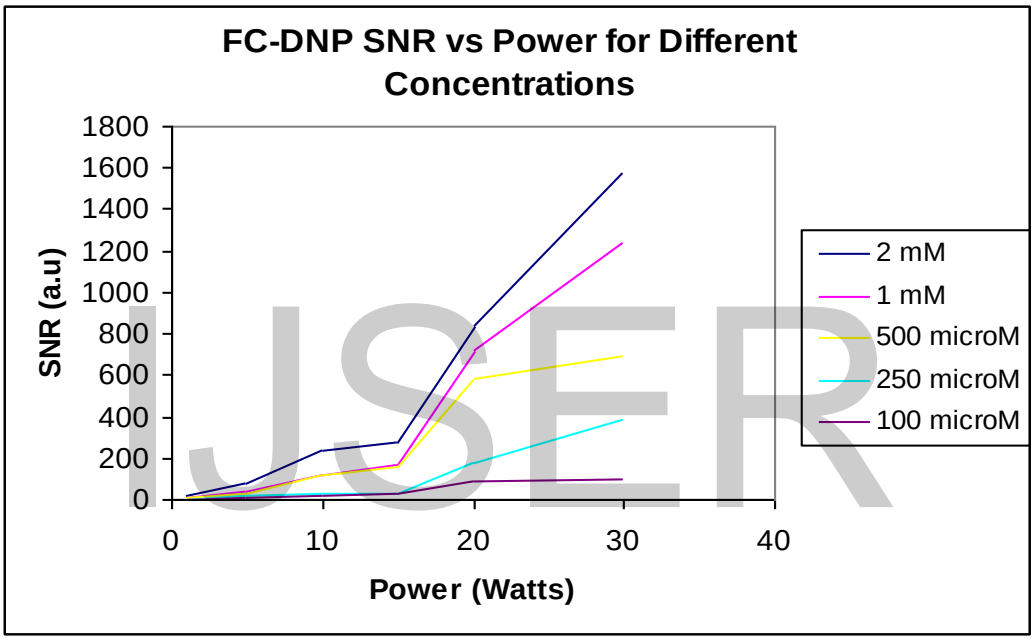

Fig 5.18: SNR versus Power for different concentrations of TEMPOL solutions.

From the figure 5.18 it is clear that the signal is proportional to the amount of concentration. The SNR values are decreased at lower concentrations.

IJSER © 2018
http://www.ijser.org

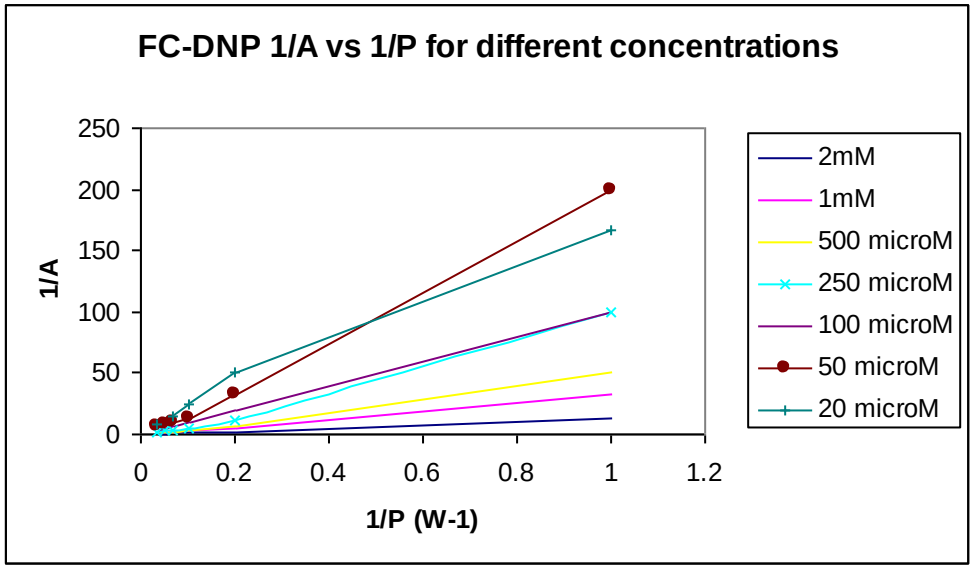

Fig 5.19: Figure showing the linear relationship for 1/A vs 1/P values.

The enhancement equation is given by the following equation 5.5:

$$\frac{1}{1-E} = \frac{n}{658\rho}\left(1+\frac{1}{\alpha\rho}\right)\left(1+\frac{1}{kCT_{10}}\right) \text{.....5.5}$$

IJSER

From the Overhauser equation the graph should be linear for 1/A vs 1/P values. And from the figure 5.19 it is clear that the power levels chosen for the experiment satisfies the condition for Overhauser effect

5.2.2 Effect of ESR Irradiation time.

ESR Irradiation Time (ms)	SNR	Overhauser Factor (A)
100	18	0.07
200	108	0.15
300	233	0.27
400	517	0.39
500	548	0.53

Table5.9: The above table shows the data for 1mM free radical sample while Power of 15 watts(Attenuation= 27dB) was kept constant.

IJSER © 2018
http://www.ijser.org

The Overhauser effect is increased and at the same time SNR of the spectra is also increased as the ESR irradiation time is increased which can be seen clearly from the charts in the figure 5.21 and figure 5.20 respectively. This effect was also observed for the rest of the low free radical concentration samples. The table 5.9 gives the parameters varied and also the results obtained i.e. SNR and the Overhauser factor for 1mM concentration.

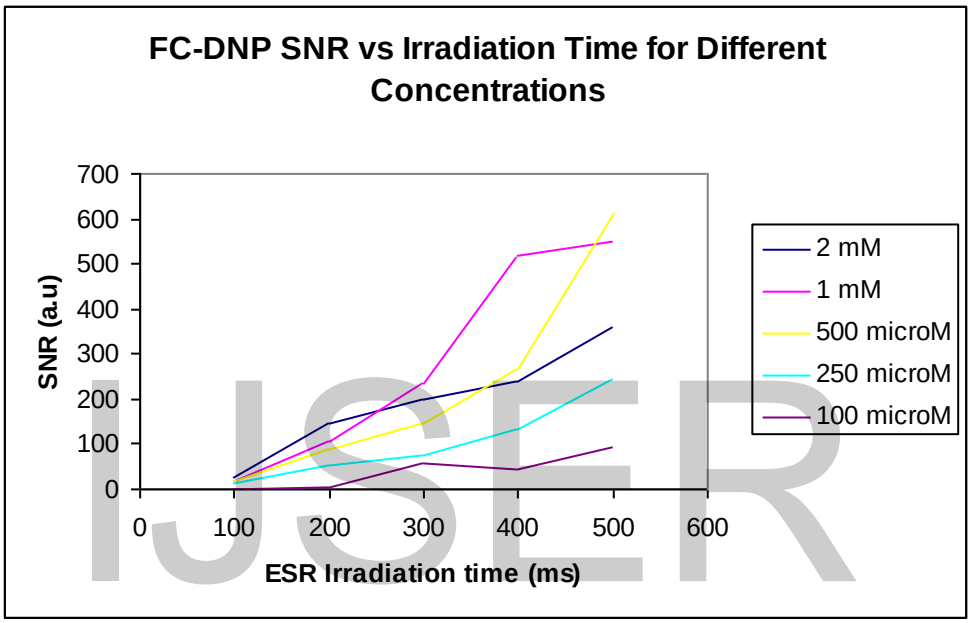

Fig 5.20: Figure showing effect of ESR irradiation time on SNR.

The figure 5.20 clearly shows that the SNR is proportional to the ESR irradiation time. The SNR is higher for higher concentrations, which is very much clear for the above graph. But the Overhauser effect is reduced for the lower free radical concentration, showing the less presence of the number of the free radical concentration in the sample, which contribute towards the enhancement of the signal as shown in the figure 5.21.

IJSER © 2018
http://www.ijser.org

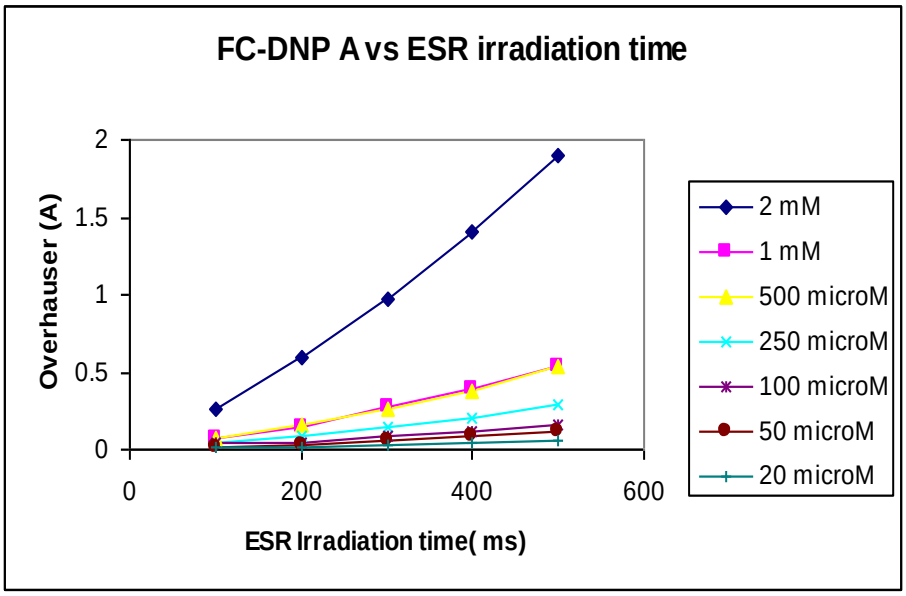

Fig 5.21: Figure showing the effect of ESR irradiation time on A.

5.2.3 Calculation of T1.

An enhancement of the NMR signal is only observed when there is free radical present in the sample. The proton relaxation is influenced significantly by the presence of the free radical. The influence of the relaxation depends on the type of the free radical and the physical environment under study.

IJSER

Parameters	**Values**
Nucleus Resonant Frequency	2.4940 MHz
Offset	4800 Hz
90 degree pulse	60 µs

Table5.10: Initial Parameters Setup for T_1 calculation experiment.

The T_1 relaxation time was measured for all different concentrations of free radical sample at a fixed magnetic field of 59mT, by employing a standard inversion-recovery pulse sequence, with a repetition time, TR, greater than five times the expected T_1 value. The initial parameters setup for the experiment is given in the table 5.10. The T_1 relaxation time was found to be increasing for the lower concentrations

IJSER © 2018
http://www.ijser.org

as seen in the figure 5.22. The T_1 values measured for different free radical concentrations are tabulated in the following table 5.11.

Concentration	T1(ms)
2 mM	672
1 mM	1009
500 microM	1383
250 microM	1658
100 microM	1913
50 microM	2055
20 microM	2125

Table5.11: Calculated T_1 values.

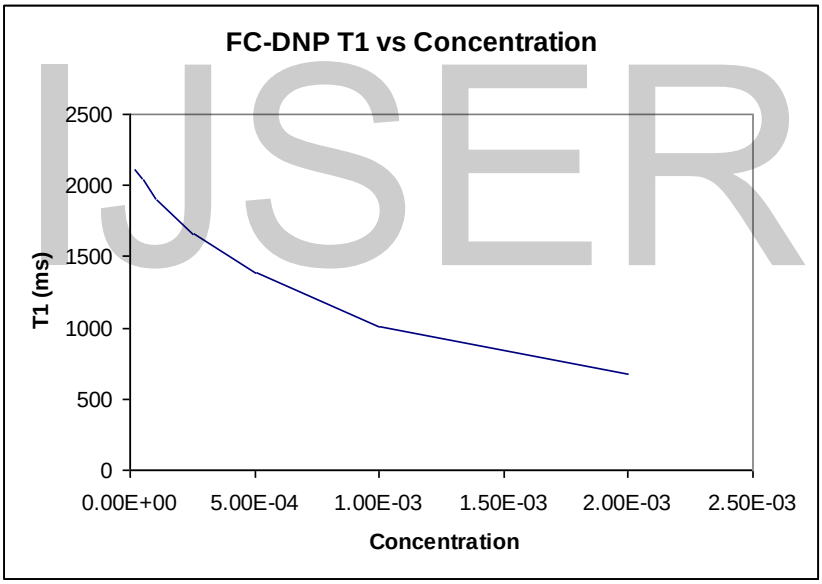

IJSER

Figure 5.22: T_1 vs. Concentration

The T_1 relaxation time of any free radical solution is given by the following equation

$$\frac{1}{T_1} = \frac{1}{T_{10}} + kC \ldots\ldots\ldots\ldots\ldots 5.6$$

Where T_{10} is the relaxation time of the solvent i.e. the spin-lattice relaxation time in the absence of any free radical and 1/kC represents the contribution to relaxation from the

IJSER © 2018
http://www.ijser.org

free radical. C is the free radical concentration and *k* is the relaxivity constant of the free radical. A plot of $1/T_1$ against C will give an intercept of $1/T_{10}$ and gradient *k* as shown in the figure 5.23.

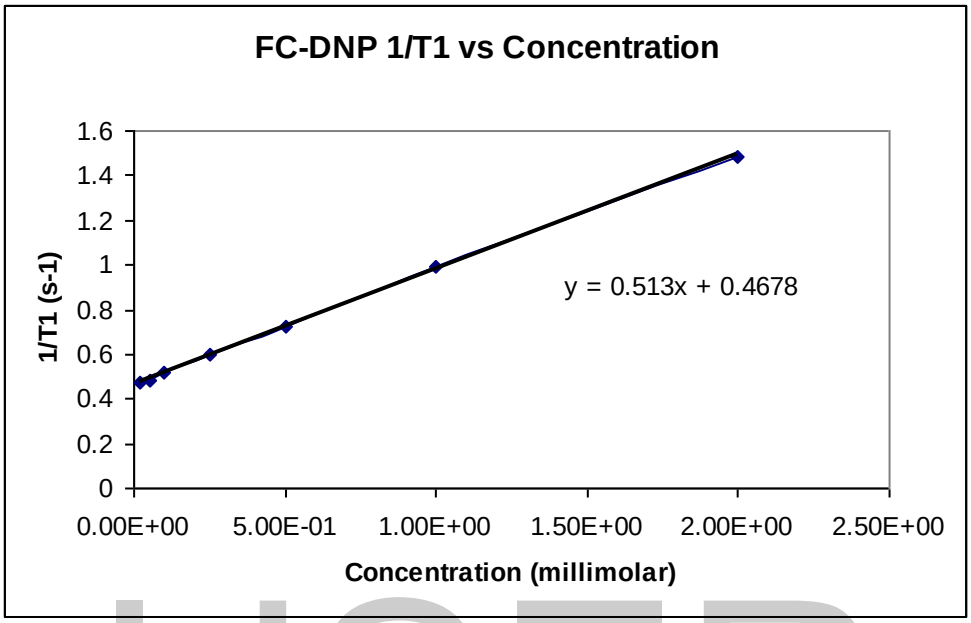

Figure 5.23 :(T_1)$^{-1}$ vs. Concentration.

IJSER

The intercept found to be is $1/T_{10}$ = 0.4678.

Hence the T_1 relaxation time for the solvent i.e. de-ionised water is 2.14 sec and the relaxitivity constant k is 0.513 $mM^{-1}s^{-1}$.

5.3 PEDRI Images

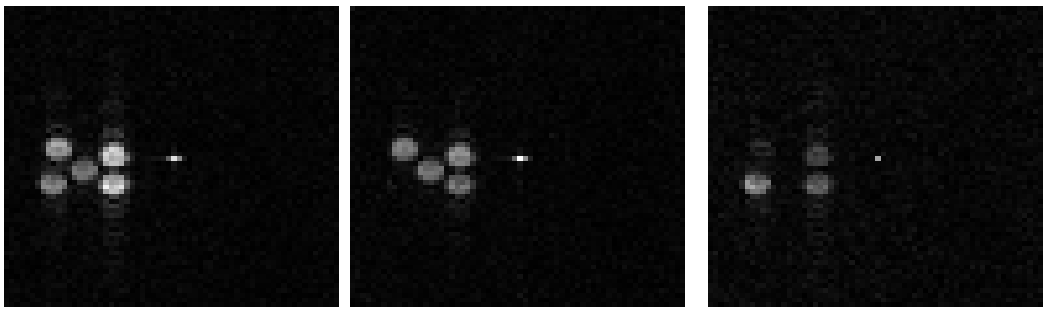

(A) EPR OFF (B) EPR ON (C) Difference Image.

Fig 5.24: The PEDRI Images obtained (A) Without EPR irradiation (B) With EPR irradiation and (C) Difference Image.

IJSER © 2018
http://www.ijser.org

The PEDRI images shown in the above figure 5.24 were obtained by placing the samples in the configuration as shown in the figure 4.10. The first image shows only the NMR intensities of the sample, since it is not EPR irradiated. Only NMR signal intensity is observed as shown in figure 5.24 (A). The second image is the image obtained with EPR irradiation and shows the Overhauser effect due to the transfer of polarisation from the electrons to the protons which appears as a dark , indicating that a negative enhancement has been produced i.e. the phase of the NMR signal is negative with respect to that in the without EPR image. As shown in the figure 5.24 (B). The NMR enhancement depends on the strength and homogeneity of the EPR irradiation field. The enhancement can only be seen in regions where the magnitude of the EPR field is sufficient to cause the Overhauser effect and only in regions where the EPR field is perpendicular to the NMR field. The difference image shows only the presence of the free radical in regions where the Overhauser effect is maximum From the figure 5.24 (C) we can clearly see the presence of free radical in the sample, where the 2mM concentration sample shows the highest signal intensity of free radical sample.

IJSER

5.3.1 Calculation of SNR.

The SNR of an image is defined as the ratio of the S_0 i.e. the mean pixel value in the region of interest (ROI) of the image to the σ i.e. the standard deviation of the noise in the image which is expressed in the following equation 5.7.

$$\text{SNR} = \frac{S_0}{\sigma} \quad \text{……..5.7}$$

IJSER © 2018
http://www.ijser.org

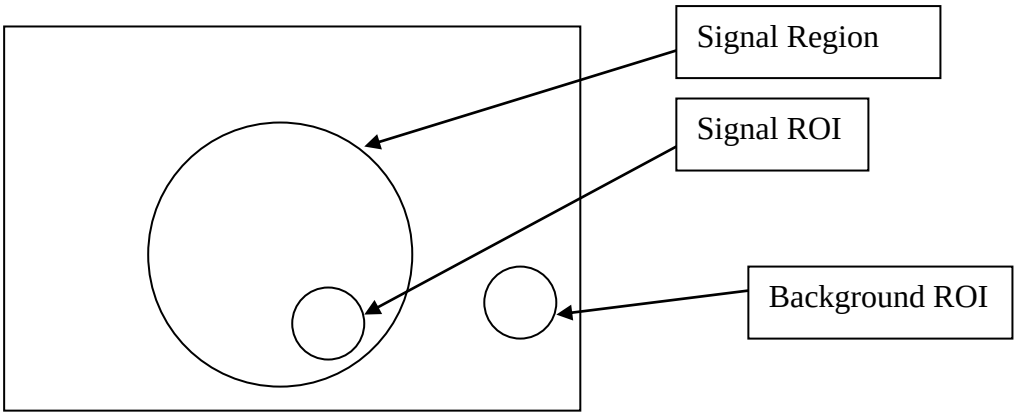

Fig 5.25: Region of Interest (ROI) of Signal and Noise in an image.

Figure 5.25 gives the general idea for the measuring the signal and noise from the image. The Fourier transformation of the k-space data of NMR gives the complex image. An MRI image is a magnitude image formed by taking the magnitude of the real and imaginary parts of this complex image. The result of this is that the noise in the background, in the absence of the signal can vary about its mean value of zero, and this affects the standard deviation measured in the noise ROI. This problem can be overcome by using a correction factor in the formula for SNR given in equation 5.3 which can be rewritten as in the following equation 5.8. [18]

IJSER

$$\text{SNR}= \frac{0.655E(S)}{SD(N)} \text{ ……..5.8}$$

Where E(S) is the mean pixel value in the signal ROI and SD (N) is the standard deviation of the pixel values in the signal ROI.

Alternatively the SNR is given as,

$$\text{SNR}= \frac{1.253E(S)}{E(N)} \text{ ……..5.9}$$

Where E (N) is the mean pixel value in the noise ROI.

IJSER © 2018
http://www.ijser.org

Samples	**E(S)**	**SD (S)**	**E (N)**	**SD (N)**	**SNR**
250 microM Tempol	523	223	153	91	**4**
500 microM Tempol	1284	86			**10**
1 mM Tempol	1857	230			**15**
2 mM Tempol	2572	432			**21**
$CuSO_4$	195	66			**2**

Table 5.12: The mean and standard deviation values of pixels in the signal ROI and noise ROI and the corresponding SNR values obtained for the difference image.

As we see from the above table 5.12, the 2mM solution has highest signal intensity compared to the other samples. The values in the above table correspond to the signal intensity. The calculated SNR values are tabulated in the above table 5.12 and from these values it is clear that the 2mM solution has got higher free radical concentration and the 250microM concentration has got the least free radical concentration.

IJSER

IJSER © 2018
http://www.ijser.org

5.4 DISCUSSION.

Both the Bruker ESR system and PEDRI system were clearly able to detect the 2mM TEMPOL solution. The minimum concentration detectable by the Bruker ESR system was 0.01 μM, compared to the 20 μM solution that could be detected by the PEDRI system. The tables 5.13(A) and 5.13 (B) give the measured SNR values at low concentrations of TEMPOL using the ESR and PEDRI systems respectively.

Tempol Solution	SNR
10 μM	2233
1 μM	234
0.2 μM	46
0.05 μM	15
0.02 μM	8
0.01 μM	3

(A)

Tempol Solution	SNR
250 μM	381
100 μM	91
50 μM	5
20 μM	3

(B)

Table 5.13: The SNR values measured at low TEMPOL free radical concentrations for (A) The Bruker ESR system and (B) The PEDRI system in FC-DNP mode.

The Bruker ESR system sensitivity depends on various parameters like Attenuation, Gain, Time Constant (TC), Conversion Time (CT) and Modulation Amplitude (MA). For example for the smaller concentrations like 0.01 μM the sensitivity was improved by increasing the values of the TC and CT values. But all the parameters have certain limits beyond which the signal may be distorted or saturated. In PEDRI the SNR of the ESR spectra mainly depends on the ESR irradiation time and the ESR irradiation power. The ESR system showed inconsistency in its performance as explained in

IJSER © 2018
http://www.ijser.org

section 5.1.6 and reproduced in the following figure 5.26. This was most likely due to the difficulty of replacing the sample (in the flat cell) in previously the same position, which in turn affected the tuning and matching of the cavity.

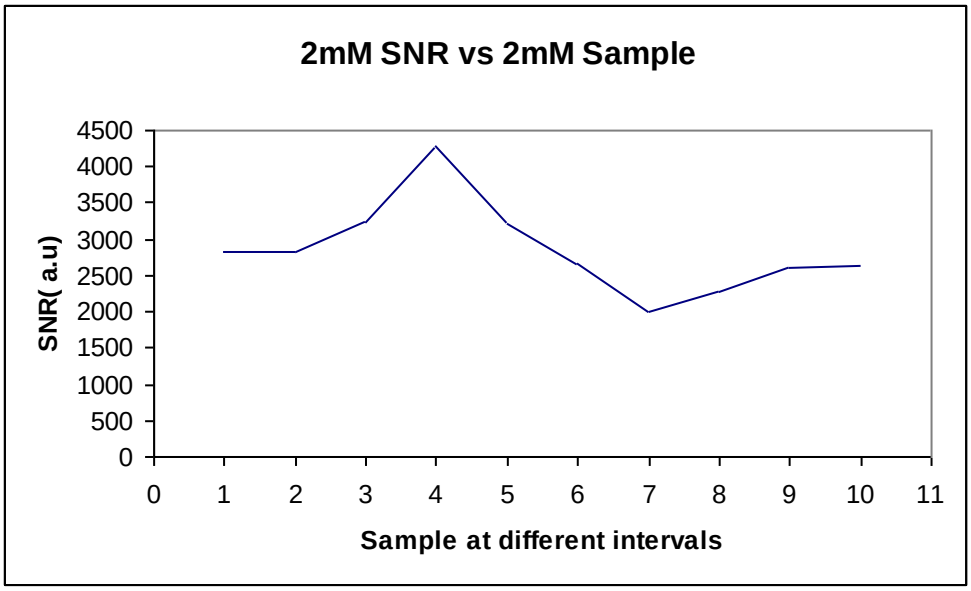

IJSER

Figure5.26: Inconsistency of the ESR Bruker system.

The irradiation frequency used in Bruker ESR system was around 9.8 GHz i.e. in microwave region, compared to 121.5 MHz used in PEDRI system. It is therefore expected that the ESR system should be significantly more sensitive than the PEDRI/FC-DNP system, and this was found to be the cost.

Figure 5.27 gives a clear comparison of the sensitivity of both the Bruker ESR system and the PEDRI system. We can clearly see that the Bruker ESR system has shown much better sensitivity compared to the PEDRI system.

IJSER © 2018
http://www.ijser.org

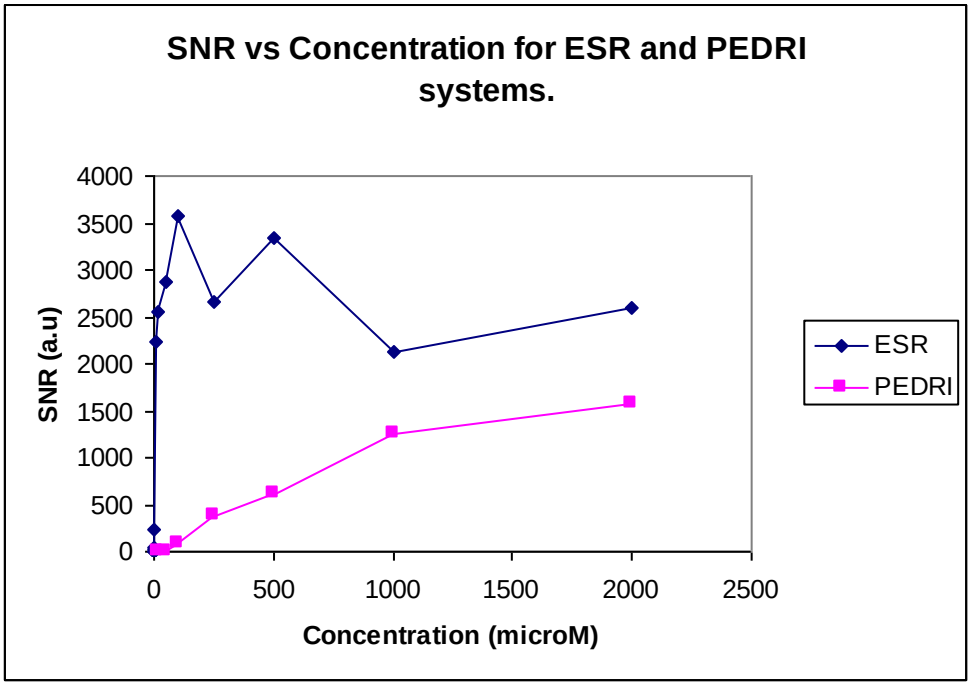

Figure5.27: SNR vs Concentration for ESR and PEDRI system.

From table 5.13 the minimum detectable concentration can be estimated by extrapolity to an SNR value of 2. This work out to be 0.0066 µM using ESR, and 13 µM using PEDRI/FC-DNP.

IJSER

Though the SNR values measured for all different samples used in PEDRI were lower than those found using ESR, the samples can be visualised or identified clearly from the PEDRI images obtained as shown in the following figure 5.28.

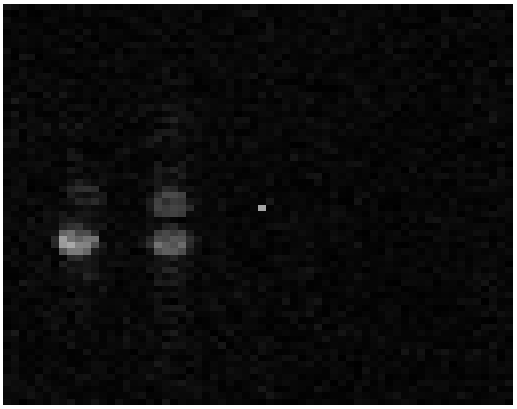

Figure 5.28: Difference image showing 2mM, 1mM, 500µM and 250µM free radical concentrations

IJSER © 2018
http://www.ijser.org

CHAPTER 6 CONCLUSION.

It is clear from the results that the sensitivity of the Bruker ESR system is much better than the PEDRI system.

The irradiation frequency used in the Bruker ESR system was much higher than the PEDRI system. The resonant power deposition in a conducting sample increases as the square of the irradiation frequency, so there is a risk of more power deposition in the samples using Bruker ESR system compared to when the samples are used in the PEDRI system. Hence the Bruker ESR system is not suitable for in-vivo experiments.

Though the Bruker ESR system was able to detect the minimum of 0.007 μM concentration compared to the 13 μM concentration detected by the PEDRI system, there is a risk of more power deposition, which we don't want. Also the Bruker ESR system shows its inconsistency in terms of producing the identical results for the sample with same parameters set compared to the PEDRI system.

IJSER

The PEDRI system is the ideal choice for studying in-vivo samples or animals, which will give enough information of the free radicals present in the samples or animals using less irradiation frequency and also provides imaging of the free radicals present. PEDRI will not be harmful for patients in case it is used for diagnosis for patients in future.

IJSER © 2018
http://www.ijser.org

6.1 Future Work.

The measurements undertaken in this project used simple solutions of TEMPOL in de-ionised water. In the future it would be useful to repeat similar measurements using solutions that more accurately reproduce the conditions that might be found in-vivo. This is especially true with PEDRI/ FC-DNP, because the NMR relaxation times of most of the samples used were considerably longer than those found in the body.

IJSER

IJSER © 2018
http://www.ijser.org

7 REFERENCES

1) Lurie, D.J., In Vivo EPR (ESR): Theory and Applications, Biological magnetic resonance, Vol.18, Edited by: L.J.Berliner, Klumer/Plenum, New York (2003).100-103,547-578.

2) Biological applications of electron spin resonance- by Harold.M. Swartz etal.

3) Electron Spin Resonance (second edition) A Comprehensive Treatise on Experimental Techniques- by Charles P. Poole.

4) Lecture Notes 2005/06, University of Aberdeen.

5) David J Lurie, Karsten Mader. (2005). Monitoring drug delivery processes by EPR and related techniques- principles and applications. *Elsevier.* 1171-1190.

6) David J Lurie etl. (1998). Design, construction and use of a large-sample field-cycled PEDRI imager. *Phys.Med.Biol* . 1877-1886.

7) D J Lurie. (2001). Free radical imaging. *The British Journal of Radiology, 74*, 782-784.

8) S J McCallum etal. (1996). A combined PEDRI and CW-EPR instrument for detecting free radicals in vivo. *Journal of Magnetic Resoncance, B 113*, 65-69.

9) M A Foster etal. (1997). The application of PEDRI to the study of free radicals.(43), 1893-1897.

10) Junichi Mizushima etal. (2000). Electron paramagnetic resonacne: A new technique in skin research. *Skin Research and Technology,* (6), 100-107.

11) Keerthi Shet etal. (2005). Proton electron double resonance inmaging of free radical distribution in environmental science applications- first results and perspectives. *ELSEVIER, 23*, 183-189.

12) THE FREE ENYCLOPEDIA, http://en.wikipedia.org.

IJSER

IJSER © 2018
http://www.ijser.org

13) Stark, D.D, Bradley, Jr W.G, "Magnetic Resonance Imaging", Vol 1, Ch 1,pp 2, 3rd edition, (1999).

14) Redpath, T W., Hutchison, JM S., " Estimating patient dielectric losses in NMR imagers", Mag.Res Imaging., 2: 295-300,(1984)

15) Prof: D. J.Lurie Lecture Notes, University of Aberdeen. 2005/2006.

16) Users Booklet for the ESR Bruker system.

17) M.A. Foster, *Magnetic Resonance in Medicine and Biology*, Pergamon Press, New York, 1984.

18) W.A.Edelstein etl. *A signal-to-noise calibration procedure for NMR imaging systems. 1983*

19) Alessandro Modrico et al. (2006). Sequential, co-registered fluorine and proton field-cycled overhauser imaging at a detection field of 59mT. *Phys.Med.Biol,* (51), N39-N45.

20) T C Christidis and F W Heinken. (1985). A cylindrical TM_{110} ENDOR cavity. *Journal Physics, 18.*

21) BRUKER BIO-SPIN PRODUCTS,

http://www.bruker-biospin.com/brukerepr/resonators.html

IJSER

IJSER © 2018
http://www.ijser.org